Ore Geology Reviews 143 (2022) 104751

Contents lists available at ScienceDirect

Ore Geology Reviews

journal homepage: www.elsevier.com/locate/oregeorev

REE residence, behaviour and recovery from a weathering profile related to the Serra Dourada Granite, Goiás/Tocantins States, Brazil

Igor V. Santana [a,*], Nilson F. Botelho [b]

[a] Universidade Federal de Minas Gerais, UFMG -Av. Pres. Antônio Carlos, 6627 - Pampulha, Belo Horizonte, MG, 31270-901, Brazil
[b] Universidade de Brasília, UnB - Brasilia, Federal District, 70910-900, Brazil

ARTICLE INFO

Keywords:
Granite weathering
Rare earth elements
Sequential leaching
Serra Dourada granite
Serra Verde Deposit

ABSTRACT

The Serra Dourada Granite (SDG) is a roughly ellipsoidal massif with batholith dimensions that crop out in Goiás and Tocantins States, Central Brazil. It has been studied since the 1970′s due to its position in a complex geological framework, and exploited by both artisanal miners and mining companies, targeting mainly cassiterite. Circa 2008–2011, it begun to be systematically surveyed in respect to its REE occurrences, culminating in the Serra Verde Deposit, a REE ion adsorption-type mineralization hosted in a reddish coarse-grained biotite granite, the first of its kind in Brazil. Given that the massif has multiple facies, this paper reports the REE residence and behaviour along a weathering profile beyond the current limits of the Serra Verde Deposit, formed at the expense of a pinkish fine-grained muscovite-biotite granite, in order to verify its potential to host a similar mineralization. It also presents the results of a 2-step sequential leaching, to assess the REE recovery from the weathered material. Monazite-(Ce), xenotime-(Y), zircon, thorite, REE fluorocarbonates and fluorite were the main REE sinks identified at the base of the profile, where the parental granite occurs. In weathered samples from horizons above, monazite-(Ce), Th-rich monazite, xenotime-(Y), thorite, Ti-bearing Fe-oxide, cassiterite, Pb-rich cassiterite, Pb-oxide and zircon were the main accessory minerals. Whole-rock analyses in the parental granite reveals REE contents of 828 ppm, and the highest grade saprolite samples yields 1,075 ppm. The chondrite-normalized REE patterns of all samples shows that the granite is LREE-selective, as well as the patterns obtained after the complete extraction. Positive Ce anomalies characterize the upper samples, whereas negative Ce anomaly characterizes horizons below. The recovery rate of the weakly adsorbed REE ions (step-1) ranges from 16 to 31%, whereas step-2 (REE associated with Fe-oxides), extracts 44–57% relative to whole rock REE. XRD analyses reveals that kaolinite and illite are the most abundant clays in weathered samples, so that those clays are the main reservoirs that adsorb REE ions released from minerals during weathering. The accumulation of the LREE in the uppermost and lower half of the profile coupled with HREE depletion, arises from the different resistance to weathering of LREE- and HREE-enriched minerals in the bedrock and saprolite. The HREE higher affinity with complexants such as OH^-, F and $CO32–$ possibly present in percolating water may also play a secondary role in leaching them out contributing the the HREE depletion. The main conclusions of this study is that easily soluble LREE fluorocarbonates provide most of the REE to the weathering profile, and that the overall REE grade in saprock and saprolite is akin to other important ion-adsorption ores, although the REE contents in leachate solutions herein are somewhat lower than others. The exception is Ce, which contents and recovery, specially following step-2, are considerable.

1. Introduction

The Serra Dourada granite (SDG) is a batholith-sized massif that crop out in mid north of Goiás and Tocantins States, Central Brazil. One of the earliest mentions to the SDG dates back to the late 1969′s (Barbosa et al., 1969), but more emphasis was given to it when the University of Brasília, cooperating with government agencies in the realm of the "Serra Dourada Project", carried out a geological survey in the area, the results being published by (Marini et al., 1977; Marini et al., 1974). It was only a decade later after its first descriptions, when (Marini and Botelho, 1986) published a study about Sn-rich granites distributed throughout Goiás State that the granite started to be evaluated in respect

* Corresponding author.
E-mail address: igor-vs@ufmg.br (I.V. Santana).

https://doi.org/10.1016/j.oregeorev.2022.104751
Received 24 June 2021; Received in revised form 31 January 2022; Accepted 1 February 2022
Available online 14 February 2022

to its metallic content, drawing the attention of the scholars to its high Sn, Nb, Zn, F, Li, Ga, U, Th and rare earth elements (REE: La-Lu + Y) contents. The knowledge built up by scholars on the granite has continued since then, marked by some key publications such as: (Bilal et al., 1997; Macambira, 1983; Marini et al., 1977, 1992; Polo and Diener, 2017; Santana et al., 2015; Teixeira and Botelho, 2006; Marini et al., 1974; Radambrasil, 1981; Santana, 2013; Ward, 2017).

Meanwhile, in China, since the 1970′s the REE have been recovered from weathered crusts developed at the expense of granitoids, forming the so-called ion adsorption-type deposits (IAD) or, as (Chi and Tian, 2008) prefer, "weathered crust elution-deposited rare earth ores". It was the beginning of the IAD contribution as an REE source, in addition, for instance, to carbonatites and heavy minerals in beach placers. The known granite's anomalous REE contents draw the attention of both scholars and mining companies, so that it begun to be economically surveyed, linking the massif to the REE industry. To date, the corporation Serra Verde Mining holds most of the mineral rights over the massif and is currently developing the infrastructure of an open pit in its southern section. The study of (Ward, 2017) focused in the current limits of the Serra Verde deposit and provides comprehensive information about it.

In IAD, the REE are not recovered directly from ore minerals such as monazite or xenotime, but either from clays formed by feldspars alteration, where the REE exist as adsorbed ions, or from secondary minerals such as REE fluorocarbonates (Bao and Zhao, 2008; Sanematsu et al., 2013; Chi and Tian, 2008). Most of the known IAD are located in the warm and humid region of southern China, distributed throughout the provinces of Jiangxi, Fujian, Hunam, Guangdong, Guangxi, Yunnan and Zhejiang (Bao and Zhao, 2008; Sanematsu and Watanabe, 2016). Other occurrences are known in southern Thailand, Laos, northern Vietnam, Madagascar and Philippines (Mentani et al., 2010; Chi and Tian, 2008; Bao and Zhao, 2008; Sanematsu et al., 2009; Sanematsu et al., 2013; Padrones et al., 2017; Estrade et al., 2019). The IAD significance arises from the fact that residual REE-clays host more than 80% of the world's resources of heavy rare earth elements (HREE; Gd-Lu + Y) (Chi and Tian, 2008), but also contribute to the light rare earth elements (LREE; La-Eu) supply to the consuming markets, justifying research on this topic.

Given the batholith dimensions of the SDG, its multiple facies and complex evolution, more research in different areas can be useful to better understand the overall formation and controls of granite-related REE mineralizations. In this respect, the purpose of this study is to verify if other areas in the massif, apart from the Serra Verde deposit, are potential to host economic REE mineralization, by assessing the local REE behaviour, supergene mobility and enrichment/depletion in its weathered products. Evaluating a weathering profile developed at the expense of muscovite-biotite granite facies, the main REE minerals are described, both in the parental granite and in its weathered products, and the results of a 2-step sequential leaching designed to recover the REE are presented. This study builds upon others cited in previous paragraphs, in which the overall REE geochemistry in the SDG have been systematically studied. The SDG hosts one of the few examples of IAD outside southern China, and the first of its kind to be surveyed in Brazil.

2. Materials and analytical methods

A weathering profile developed over muscovite-biotite granite was surveyed, from which 6 samples, labelled 20 to 25, were taken in intervals at different horizons along the profile. Whole-rock analyses of samples 20–25 were performed by ALS Global Lab. Major oxides were quantified by ICP-AES in accordance to ALS package code ME-ICP06, where 2 g of sample is converted into fused beads and submitted to acid digestion prior do analyses; reference materials are SY-4 and OREAS-45c. The REE and other trace elements were quantified by ICP-MS according to the package ME-MS81, where 2 g of sample is submitted to lithium borate fusion prior to acid dissolution and analyses; reference materials are OREAS-45c, OREAS-146 and GRE-3. The results are summarized in Table 1.

Table 1
Results of whole-rock analysis of samples 20 to 25.

Sample #	20	21	22	23	24	25
Oxide (wt%)						
SiO_2	56.3	72.6	73.5	75.4	75.8	76.4
TiO_2	0.51	0.23	0.23	0.26	0.25	0.18
Al_2O_3	24.4	14.9	13.7	13.2	12.7	11.4
Fe_2O_3	5.05	2.26	2.22	2.11	2.42	1.77
MnO	0.01	0.01	0.01	0.01	0.01	0.01
MgO	0.26	0.07	0.09	0.14	0.44	0.35
CaO	0.02	0.02	0.02	0.04	0.03	0.67
Na_2O	0.21	0.29	0.32	0.35	0.47	2.83
K_2O	2.95	4.34	4.81	5.61	6.15	5.14
P_2O_5	0.02	0.01	0.01	0.02	0.01	0.01
LOI	10.7	4.72	3.85	2.96	2.56	0.6
Total	100.4	99.5	98.8	100.1	100.9	99.4
(ppm)						
Th	158.50	99.70	92.10	76.30	100.00	70.50
U	19.55	10.60	9.57	8.81	5.29	8.31
Nb	63.70	31.90	32.70	33.60	29.20	25.20
Zr	533.00	338.00	308.00	363.00	337.00	328.00
Sn	205.00	41.00	39.00	35.00	69.00	45.00
Y	86.80	58.70	61.40	53.10	64.20	113.00
La	181.50	95.10	148.50	251.00	208.00	201.00
Ce	581.00	303.00	259.00	503.00	336.00	269.00
Pr	35.40	18.30	28.80	48.80	40.30	36.70
Nd	113.00	58.20	88.00	148.00	133.00	122.00
Sm	17.90	8.78	13.35	23.50	23.10	21.50
Eu	0.70	0.40	0.69	0.86	0.93	0.82
Gd	15.55	8.82	12.15	16.35	18.40	20.10
Tb	2.44	1.49	2.05	2.47	2.66	3.11
Dy	15.20	10.50	12.60	12.55	13.60	17.60
Ho	3.36	2.37	2.72	2.23	2.52	3.41
Er	9.17	7.27	7.85	5.68	5.68	9.07
Tm	1.44	1.13	1.26	0.90	0.83	1.32
Yb	9.59	8.05	8.17	5.98	5.25	8.34
Lu	1.33	1.19	1.07	0.79	0.78	1.24
LREE	928.80	483.38	537.65	974.30	740.40	650.20
HREE	145.58	99.92	109.96	100.91	114.85	178.01
REY	1074.38	583.30	647.61	1075.21	855.25	828.21
Ce/Ce*	1.74	1.75	0.95	1.09	0.88	0.75
Eu/Eu*	0.13	0.14	0.17	0.13	0.14	0.12
(La/Yb)CN	12.76	7.96	12.25	28.30	26.71	16.25

$Ce/Ce^* = CeN/(LaN \times PrN)1/2$
$Eu/Eu^* = EuN/(SmN \times GdN)1/2$

Carbon-coated thin sections of the parental granite (sample 25) and resin blocks of the weathered samples above were submitted to scanning electron microscopy (SEM) in order to generate back-scatter electron (BSE) images. It was performed using a Jeol JSM-6510, with 20 kV acceleration voltage in high vacuum mode.

X-ray diffractometry (XRD) analyses were performed using a Panalytical X'pert PRO MPD x-ray diffractometer. For bulk samples, the random powder method was used, the scanning set continuous from 5 to 70° 2 θ, with 0.02° 2 θ step and exposure time of 0.5 s per step. The clay-sized fraction was separated by initial centrifugation at 750 rpm for 8 min, and again at 3000 rpm for 30 min. The oriented clay aggregate was produced by smearing the obtained clay paste on glass slides, dried at room temperature and scanned from 5 to 32° 2 θ, at a scan speed of 0.025 °/s. A current of 40 mA and tension of 45 kV were set to produce the x-rays.

The pH of samples was measured with pH 4.0–7.0 test strips and therefore is semiquantitative. For the readings, the paper tests were dip in the humid sample until no color change was observed, and compared with a color template with known pH values.

2.1. Sequential leaching

To date, one of the most applied techniques to recover the REE

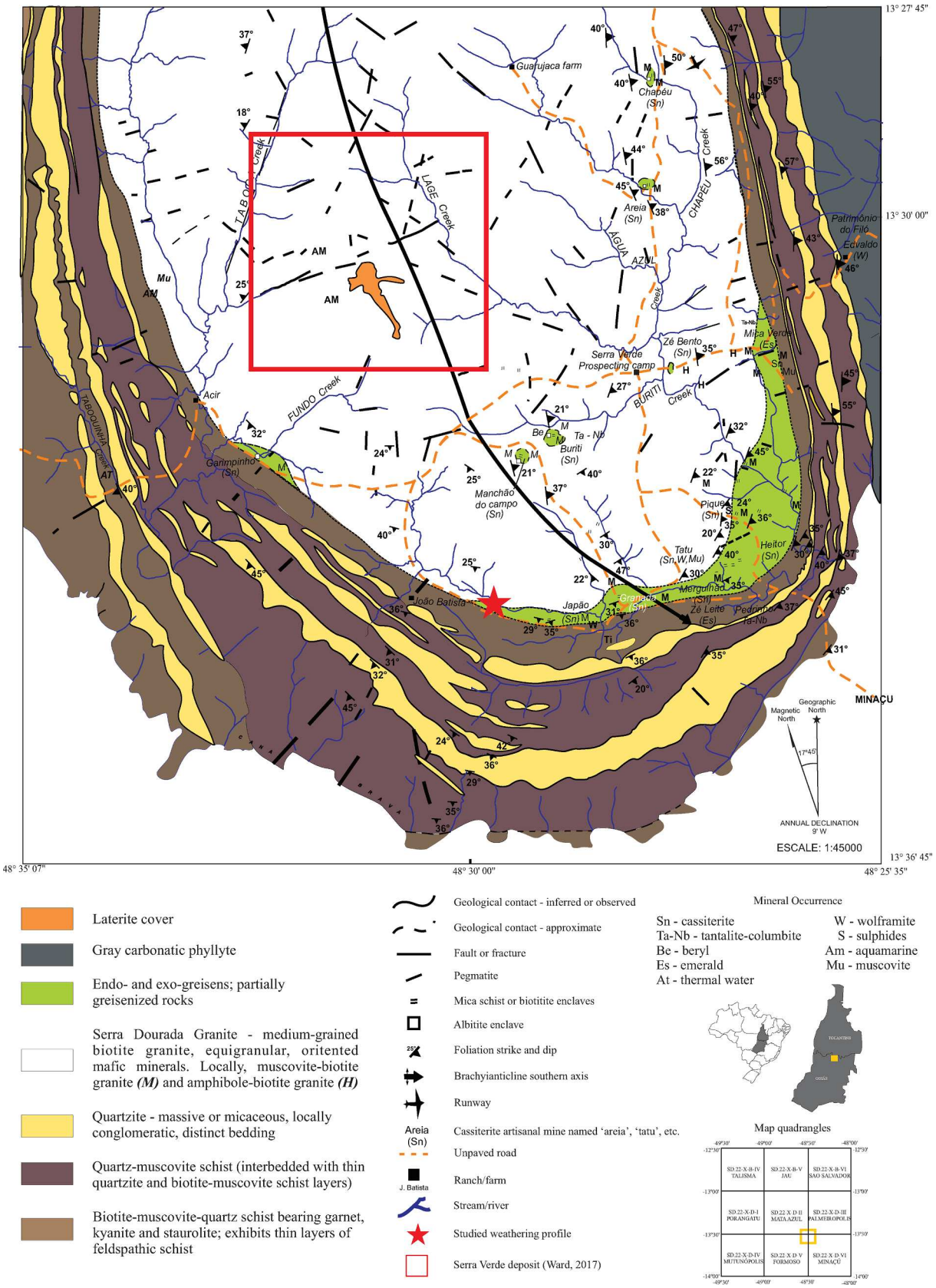

Fig. 1. Geological map of the southern border of the Serra Dourada granite. Modified version of the original printed map produced and reported by (Macambira, 1983). Refer to (Ward, 2017) for precise information on the Serra Verde Deposit.

consist in ion-exchangeable reactions and leaching steps with reagents that dislodge the REE from their host materials. In this study, the leaching was performed following the procedure described by (Sanematsu et al., 2013), which is based in the Community Bureau of Reference (BCR) of the European Commission modified and improved by (Ure et al., 1993; Thomas et al., 1994; Rauret et al., 1999). The leaching was carried out in the wet-chemistry lab of Camborne School of Mines (CSM), UK.

Step 1 aimed the recovery of weakly adsorbed ions retained on the surface of mineral particles, mainly clays, by means of ion-exchangeable reactions. A 40 ml volume of 0.5 M ammonium sulphate solution adjusted at pH = 4 with H_2SO_4 was added to 1 g powder sample in centrifuge tubes. The solution was left to react with the powder sample overnight (approximately 16 h) in an end-to-end shaker at room temperature. The solid and liquid phases were separated by centrifugation for 20 min, and the resulting supernatant solution was filtered under vacuum through a 0.22μ m membrane filter into polyethylene containers. The filtration apparatus was rinsed with 50 ml distilled water, and the final solution was acidified with 5 ml HNO_3. This process culminates in 95 ml REE-bearing solution (40 ml reagent + 50 ml distilled water + 5 ml HNO_3) stored in the polyethylene containers, kept under refrigeration before being submitted to ICP-MS. The solid residue left in the centrifuge tubes was submitted to a second leaching step.

Step 2 targeted the recovery of REE bound to Fe,Mn-oxides. A 40 ml volume of 0.5 M hydroxylammonium chloride adjusted to pH = 2 with HNO_3 was added to the step 1 solid residue, further submitted to the same processes of centrifugation and filtration described in the previous paragraph.

The REE content in the leachate solutions was quantified using an ICP-MS located in the same institution, using the reference material IV-ICPMS-71A produced by *Inorganic Ventures* to generate the 1.6, 8, 40, 200 and 1,000 ppb calibration curves. For each individual sample three replicates were made, totalizing 4 runs per sample per step, so the average REE contents was considered. The obtained results, in ppb, were multiplied by the dilution factor of 95 and converted to ppm to get the final number. The REE content in the solid residue was calculated simply by subtracting the extracted REE from the whole rock REE reported in Table 1. Internal CSM lab numbers are C08150232 to C08150255 for step-1, and C08150399 to C08150422 for step-2.

3. Serra Dourada granite

The SDG (Fig. 1) sits within the northern domain of the Brasília fold belt (BFB), central Brazil, an orogen formed in the early Neoproterozoic Gondwana assembly, as a result of the amalgamation of the Amazon and São Francisco cratons along with a third block, currently underneath the Paraná Basin (Marini et al., 1984; de Brito Neves et al., 1999; Dardenne, 2000; Valeriano et al., 2008). Despite its current placement, the granite was formed previously the BFB, and is actually considered anorogenic. According to (Bilal et al., 1997), the SDG was formed during the first extensional event post-dating the Transamazonian Orogeny. The most reliable geochronological data available were not carried out directly in the SDG but in correlated massifs, namely the Sucuri, Soledade and Serra da Mesa Granites (Pimentel et al., 1991). That author reports U-Pb zircon age for the Sucuri and Soledade massifs of 1767 ± 10 Ma and 1769 ± 2 Ma, respectively; the Serra da Mesa is ca. 150 Ma younger than those two.

It forms a roughly 8-shaped massif with batholith dimensions, with approximately 55 km length and 13 km width at its broader section. Along with other correlated oval-shaped massifs, namely, Serra do Encosto, Serra da Mesa and Serra Branca Granites, encompass a series of REE, Sn-mineralized granitoids that crop out in mid north Goiás State, Brazil. The massifs, specially the SDG, stand out in the region as high topographic terranes, contrasting with their surrounding geological units of the Serra da Mesa Group. That group is described as a succession of muscovite-bearing quartzitic and *meta*-psammopelitic facies (mainly mica schist) with interlayered calcischist and both marble lens (Marques, 2009). Saccharoidal quartzite layers form the sharp crests in direct contact with the granite itself, delineating most of its outer limits.

The earliest mention to the SDG dates back to the late 1960's, when (Barbosa et al., 1969) described it as a dome of grayish to pinkish coarse-grained granite-gneiss, with oriented micas and microcline as the dominant feldspar. Later, (Marini et al., 1974) provided more information on the granite's overall features in the realm of the "Serra Dourada Project" – a joint effort between the University of Brasília and the National Mineral Production Department to contribute with the understanding of the Precambrian framework at Goiás State. Those authors noticed the strong foliation, the occurrence of pegmatite, migmatite and gneiss at the granite borders. Furthermore, they emphasized the SDG importance, especially at its southernmost section, due to fluorite enrichment and economic concentrations of colluvial cassiterite. This locality is known until today as Pela Ema Mine, intensely exploited by artisanal miners during the 1980's, but currently inactive. Further details were given by (Marini et al., 1977), who added descriptions from inwards the massif such as the occurrence of banded gneiss with migmatitic structure and amphibolite, the latter probably as representative of former basic dykes. They also reported remnants of schist in the eastern and northern parts of the massif. The SDG was also studied under the umbrella of the "RadamBrasil Project" (Radambrasil, 1981). It was a comprehensive survey carried out in Brazil by means of radar image acquisition, in order to evaluate the National natural resources such as geology, vegetation, land use, among others. In the relevant section regarding the SDG (p. 146), the authors report basically the same features already observed by others, but add its hypabyssal nature and the occurrence of greisenization, suggestive of late-stage metasomatic processes.

The scholars and studies aforementioned approached the general features of the SDG, but it was (Macambira, 1983) who systematically evaluated the associated mineralization in its southern portion, including the neighboring country rocks of the Serra da Mesa Group. At that time, artisanal miners were already flocking in the area in order to exploit cassiterite, beryl, muscovite and gold (the latter not intrinsically related with the granite itself) and mining companies such as METAGO and Goiás Estanho SA were also active in the region, mostly interested in cassiterite with tantalite-columbite and wolframite as byproducts. In addition to the cited commodities, (Macambira, 1983) also reported the occurrence of monazite, kaolin, chalcopyrite, topaz, rutile, thermal water, amazonite, garnet, kyanite and staurolite.

Over the next few years, the knowledge on the metallic content and economic importance of SDG (and other granites) were enhanced by the study of (Marini and Botelho, 1986). They assessed not only the SDG but about two dozen of related granitoids, most of which Sn-mineralized, having coined the term "Goiás Tin Province" (GTP). According to those authors and to (Marini et al., 1992), it exhibits overall features such as conspicuous foliation, especially on its borders, and rock-forming minerals represented by large microclinized feldspars, quartz, biotite and, more rarely, hornblende. They report ilmenite, zircon, apatite, titanite and allanite as the commonest accessories, and late to post-magmatic alteration such as microclinization, albitization and greisenization. According to them, the studied granites have characteristics of both A and S-types.

(Marini et al., 1992) main contribution was the evaluation of the SDG in terms of REE. They analyzed 06 samples, including the biotite granite, biotite-muscovite granite and albitite, which averaged 888 ppm, with highest contents of 1,713 ppm yielded by albitite from the Pela Ema Mine. Still according to them, the chondrite-normalized REE patterns are predominantly descendent [(La > Lu)cn] with negative Eu anomaly. The study of (Bilal et al., 1997) also enhanced the understanding of the granite itself and its associated mineralization in its northwestern limits. Those authors reported three main lithotypes: amphibole-biotite granite at the massif border, biotite granite as the main facies and a more evolved fine-grained porphyritic granite

Table 2
Consulted references of studies carried out in the SDG.

References	Samples
RadamBrasil (1981) p.148	110; 107; 108; 111.1
(Macambira, 1983) p.53	1 to 6
(Marini et al., 1992) p.65	PE-1; MA-2; PE-6; MA-1; PE-2; PE-3
(Bilal et al., 1997) p.360	Amphibole granite, biotite granite, porphyritic granite
(Teixeira and Botelho, 2006) p.682	SD09A; PE6; SD09B; SD09C; SD24A; SD24G; SD24E
Polo and Diener, 2017 p.144	HP62B; HP310; HP344; HPR63; HPR54; HP349A; HP351; HP350; HP362A; HPR62; HPR100; HP311; HPR101
(Santana et al., 2015) p.12	FG1; FG2; FG3
Ward (2017) p. 112–113	All samples reported in pages 112–113.

crisscrossing the main facies. They classify the SDG as A-type derived from continental crust, based in the high Th, Nb, REE + Y contents, relatively low CaO, P_2O_5 and Sr contents, low MgO/TiO_2 and Zr/Nb, and high 10000 Ga/Al ratio. (Teixeira and Botelho, 2006; Teixeira, 2002) went further in assessing the REE residence and their geochemical behaviour coupled with the magmatic/hydrothermal evolution of the SDG. REE contents reported in that study average 701 ppm, with highest contents from an albitite sample with 1,144 ppm. The authors mention apatite, allanite, monazite, bastnäsite, REE-oxyfluorides, fluocerite, zircon and xenotime as the minerals responsible for the REE contents in the granite, which increases following alteration processes such as albitization and biotitization. Thorite was not observed by them, but (Santana et al., 2015) could detect it in SEM-EDS analysis carried out in biotite granite with minor hornblende. Three samples of the fresh biotite granite analyzed by them yielded 613, 619 and 826 ppm REE.

Around 2008–2011 the SDG started to be surveyed by private companies targeting its REE enrichment associated with the granite's weathered products. The company Serra Verde Mining holds most of the mineral rights over the massif, and is currently developing an open pit mine on the granite's southern border. (Ward, 2017) carried out a detailed research on the deposit area, hosted by a red foliated coarse-grained feldspar-quartz-plagioclase-biotite granite. A plethora of REE minerals were reported in the deposit such as bastnäsite-(Ce), bastnäsite-(La), samarskite-(Y), pyrochlore, yttro-columbite, aeschynite, fergusonite, fluorobritholite-(Ce) and fluorobritholite-(Y), in addition to others in weathered granite samples.

4. Geochemistry

Previous studies carried out in the SDG were consulted to build up a set of whole rock chemical data. The Table 2 condenses the consulted references and the samples considered. Only a limited number of studies reports both major oxides and REE; some report only major oxides, others only the REE. Rare Si-undersaturated rocks do occur within the granite domain, as natural counterparts of the main granite but, in general, only samples representative of fresh granitoids were considered. Table 3 summarizes the highest, lowest and mean values for major oxides and REE found in the consulted references.

The chemical data portray high SiO_2 contents, average 73.8 wt%, ranging from 65.9 to 78.3 wt%. The alumina contents range from 10.1 to

Table 3
Summarized statistical parameters of reported SDG chemical analyses.

	SiO_2	Al_2O_3	Fe_2O_3	CaO	Na_2O	K_2O	MgO	TiO_2	P_2O_5	LREE	HREE	REY
Mean	73.81	12.35	2.55	0.98	2.91	5.31	0.21	0.29	0.06	680.28	229.40	909.68
Min	65.90	10.10	0.01	0.34	1.80	1.15	0.02	0.09	0.01	360.54	40.40	461.10
Max	78.29	13.80	6.48	2.93	5.28	6.34	1.32	1.28	0.41	1,420.13	768.56	2,188.69

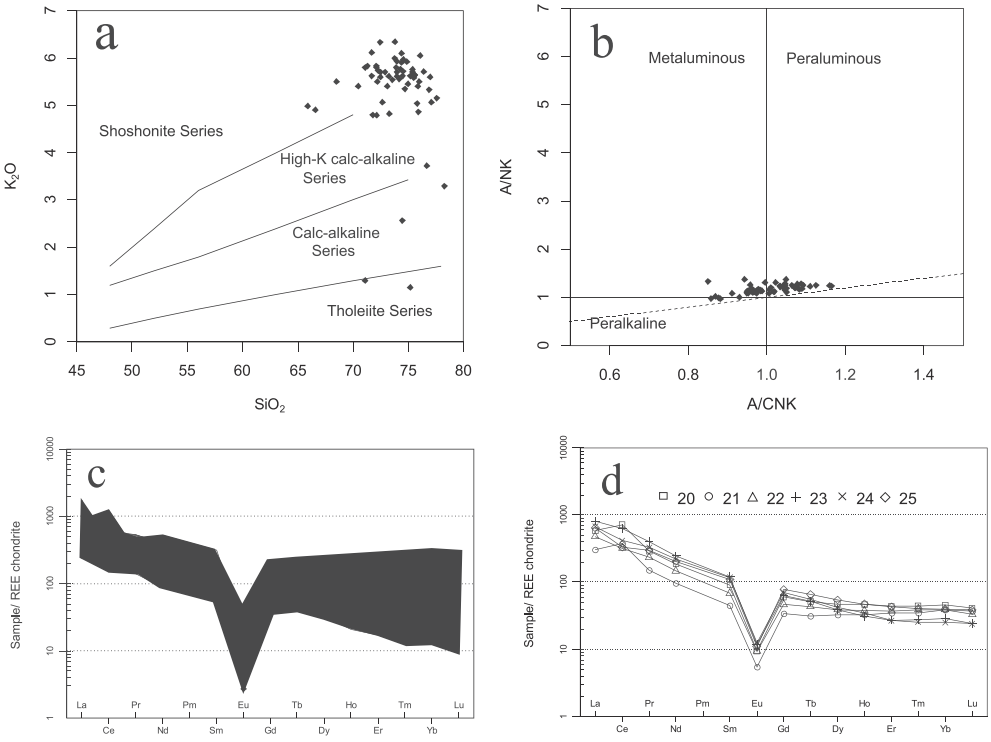

Fig. 2. a and b) K_2 O wt% vs. SiO_2 wt% (Peccerillo and Taylor, 1976) and A/NK vs A/CNK (molar) (Shand, 1943) classification plots. c) Chondrite-normalized REE patterns of the consulted references from Table 2 and d) chondrite-normalized REE patterns of samples 20 to 25. Chondrite values from (Boynton, 1984).

Profile	Horizon	Depth (cm)	Description
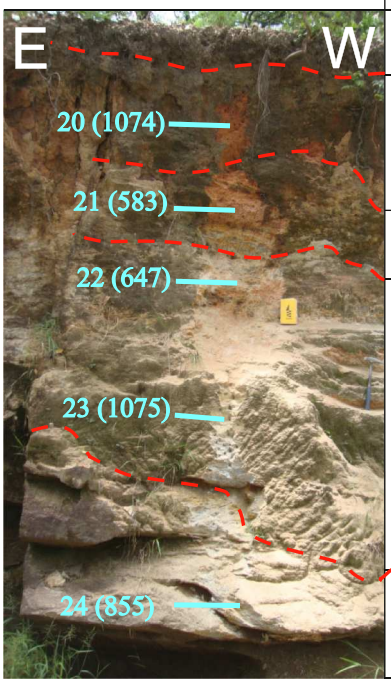	A	0 - 30	Organic matter; loose leaves and sticks; mineral fraction composed of quartz pebbles.
	B	31 - 60	Al-Fe accumulation, few roots, collumnar, vertical prismatic structures, clay-rich.
	C_1	61 - 100	Orange saprolite, interlayered with white saprolite. Granite's texture and foliation still preserved. Loose mineral particles, weathered micas, clay-rich.
	C_2	101 - 400	White saprolite, friable, micas and plagioclase relicts, clay-rich.
	C/R	Below 400	Muscovite-biotite granite saprock, foliated, pinkish hue, lower clay contents.

Fig. 3. Studied profile and samples location. Numbers in parenthesis indicate total REE contents.

13.8 wt%, averaging 12.3 wt%, and tend to be higher when SiO_2 is lower. The SDG is more potassic than sodic: K_2O average 5.3 wt%, and Na_2O average 3.1 wt% and so that most samples plot in the shoshonite and high-K calc-alkaline series (Fig. 2a). Some examples are relatively poorer in K_2O, for example sample HP62B published by (Polo and Diener, 2017), which is compensated by higher CaO and Na_2O contents. The samples were also plotted in the A/NK vs. A/CNK diagram after (Shand, 1943) (Fig. 2b) in order to compare the alumina with alkalis. About half of the samples plot in the metaluminous field, the other half exhibit a peraluminous character. The most common peraluminous rock-forming minerals are biotite, muscovite and more rarely, garnet. The Na_2O, K_2O and MgO do not exhibit a clear trend with SiO_2 variation, but CaO is higher when silica contents are lower; so are Fe_2O_3, TiO_2 and P_2O_5. The Fe_2O_3 contents range from 0.01 to 6.48 wt%, average of 2.55 wt%. The P_2O_5 contents are low, average 0.06 wt%, with some outliers up to 0.41 wt% reported in amphibole granite (Bilal et al., 1997). The

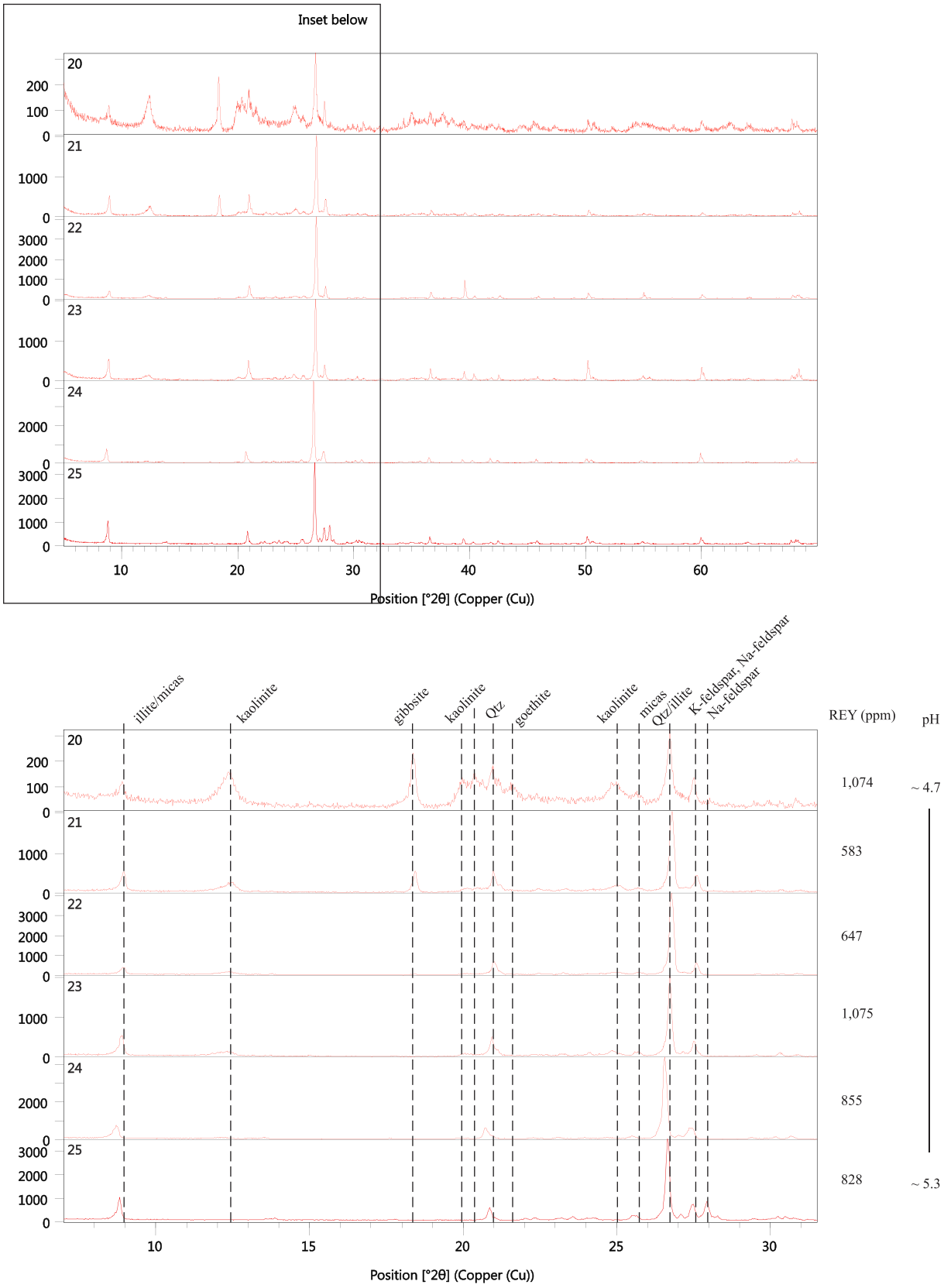

Fig. 4. Combined XRD diffractograms of bulk samples 20 and 25.

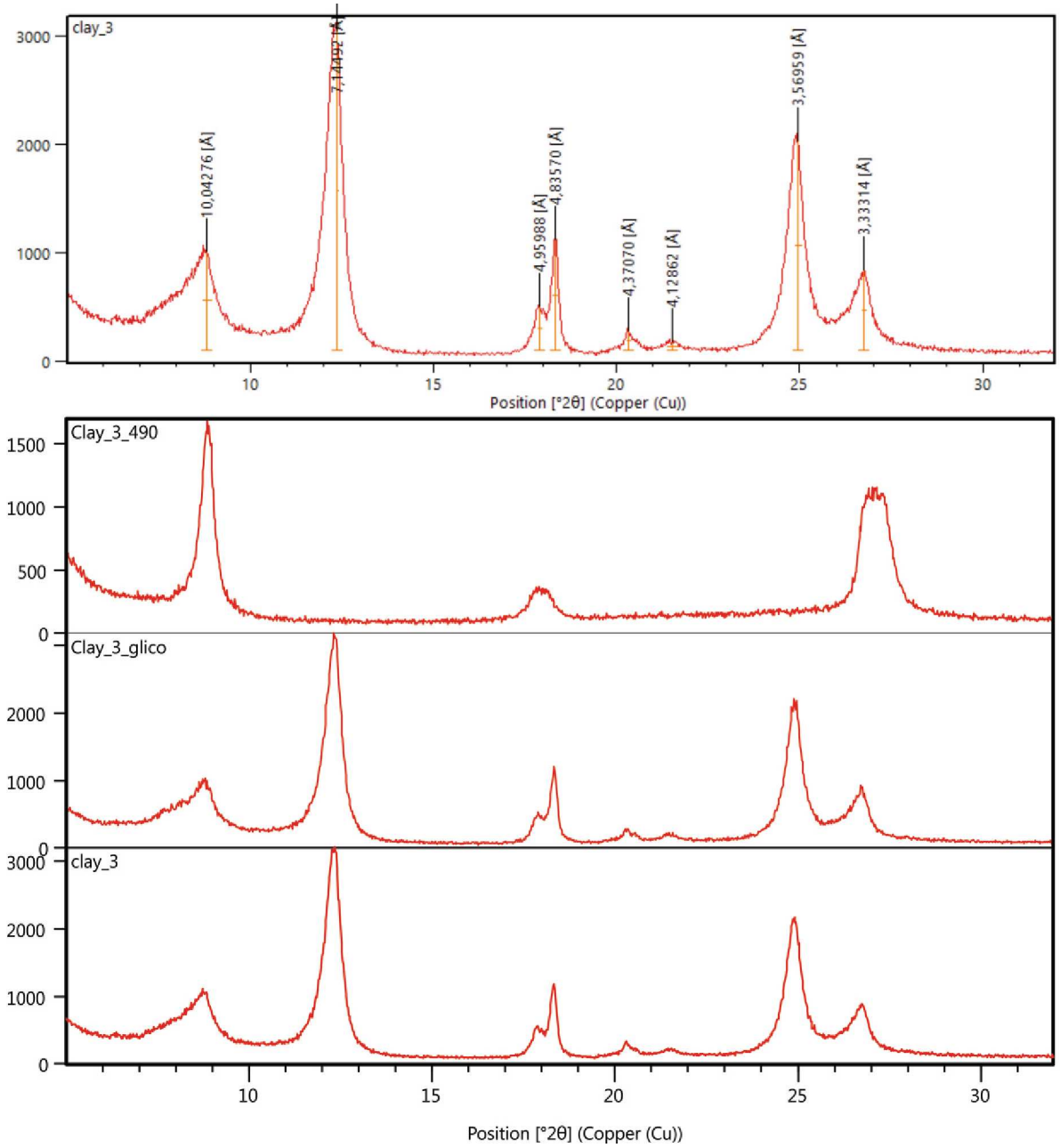

Fig. 5. Clay-sized diffractogram of sample 20 - air dried, ethylene glycol solvated and heated to 490 °C.

plagioclase relations observed in sample 25 corroborate the potassic affinity observed in literature samples, as microcline and orthoclase are more abundant than plagioclase. Syeno and monzogranite compositions embrace the vast majority of SDG samples.

Total REE contents reported in the consulted references are high, average of 900 ppm, mainly due the high grade samples of (Ward and Carmen, 2017), collected directly from the Serra Verde deposit. Overall, total REE contents range from 461 to 2,188 ppm, which is comparable to Chinese deposits. The SDG is clearly LREE-selective, as illustrated by the chondrite-normalized REE pattern in Fig. 2c, with low to moderate descendent fractionation. The HREE exhibit more variation in their own fractionation, from descendant to flat, with few samples in ascendent fractionation. Ce, La and Nd are the most abundant LREE; Y, Gd and Dy are the most abundant HREE. When combined, the LREE average 680 ppm, and the HREE 229 ppm. Fig. 2d shows the chondrite-normalized REE pattern of the original samples 20 to 25. The REE fractionation is similar of those from the references, reflecting the granite's original REE mineralogy where LREE-phases predominate. The Ce anomalies are positive in the two uppermost samples 20 and 21, and absent or negative in the remaining samples below. The negative Eu anomaly is also strong, ranging from 0.12 to 0.17.

5. Weathering profile description

The studied profile (22L 771,088 E; 8,498,197 S UTM) is located in the very southern border of the SDG, near the contact with the Serra da Mesa units (Fig. 3). It was found next to Pela Ema mine, inactive at the moment, dug by artisanal miners exploiting both detrital and albitite-hosted cassiterite enclosed by muscovite-biotite granite. There is no official information on the exposure history of the profile, but it was possibly excavated by tin miners searching for cassiterite-rich veins, as an extension of the Pela Ema mine. Although the transect is relatively low (about 5 m deep), it was the best exposure found during fieldwork, where the whole sequence, from parental granite to top soil cover are *in*

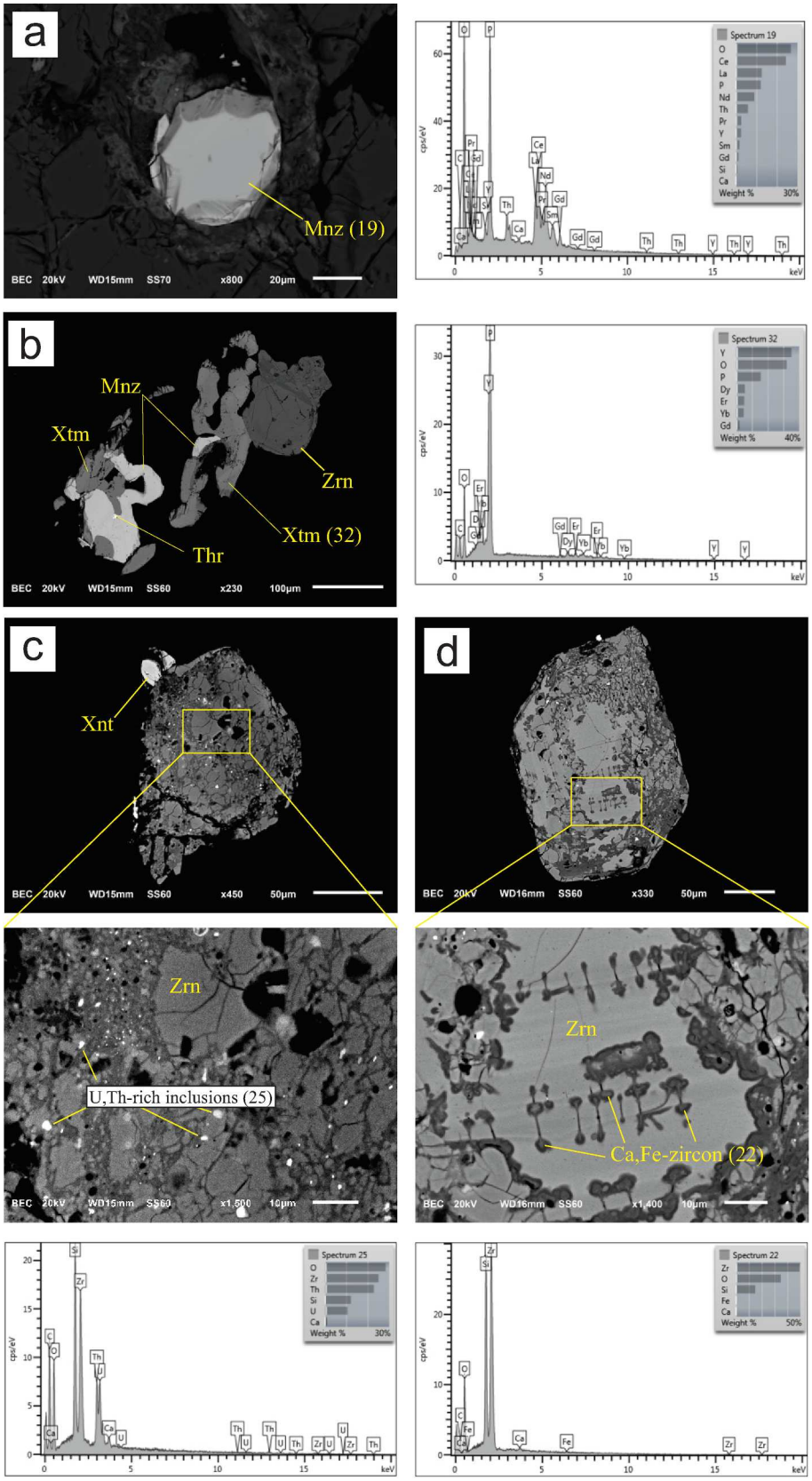

Fig. 6. SEM-BSE images of accessory minerals found in fresh parental granite. Mineral abbreviations from (Whitney and Evans, 2010).

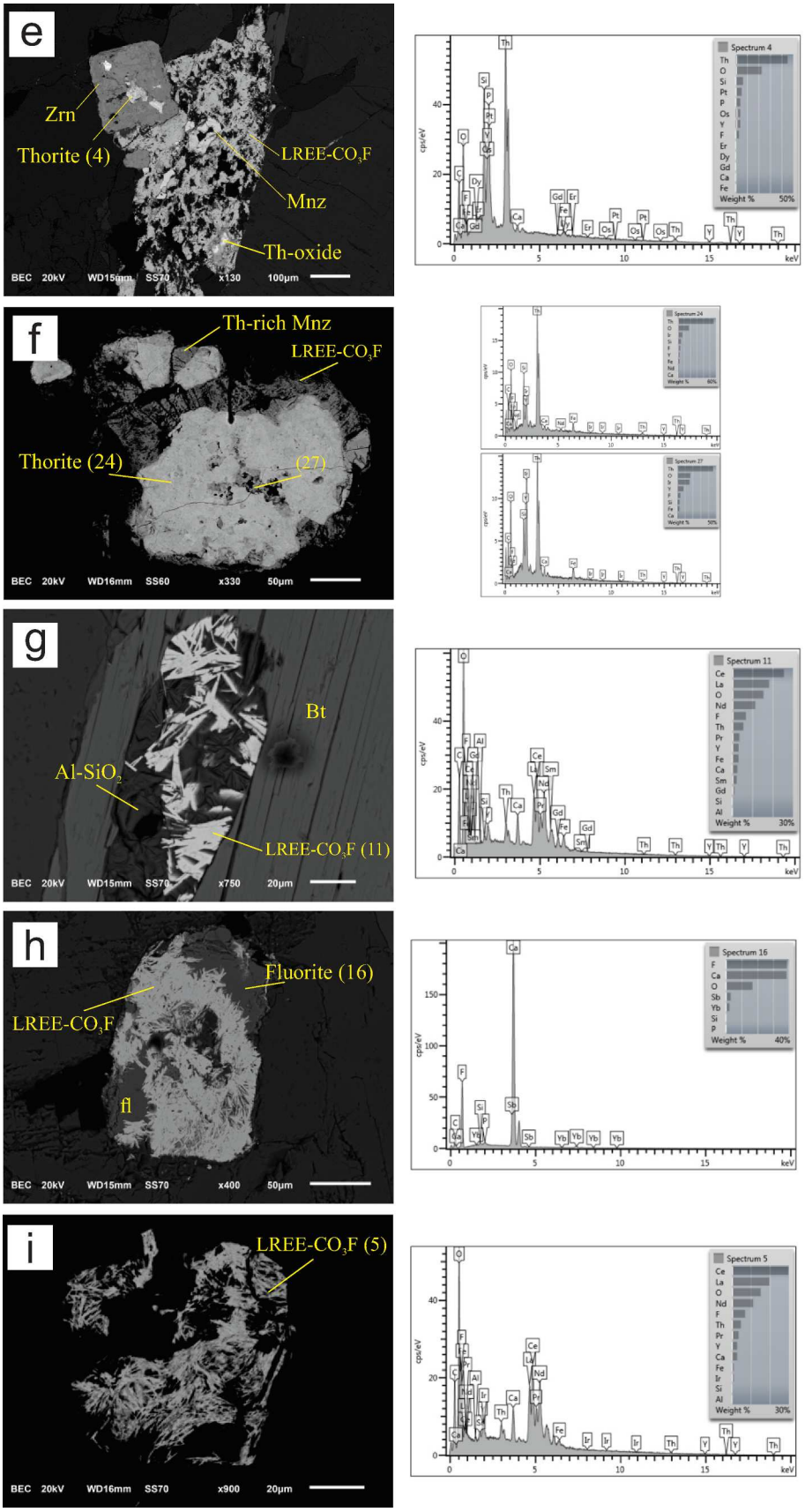

Fig. 6. (*continued*).

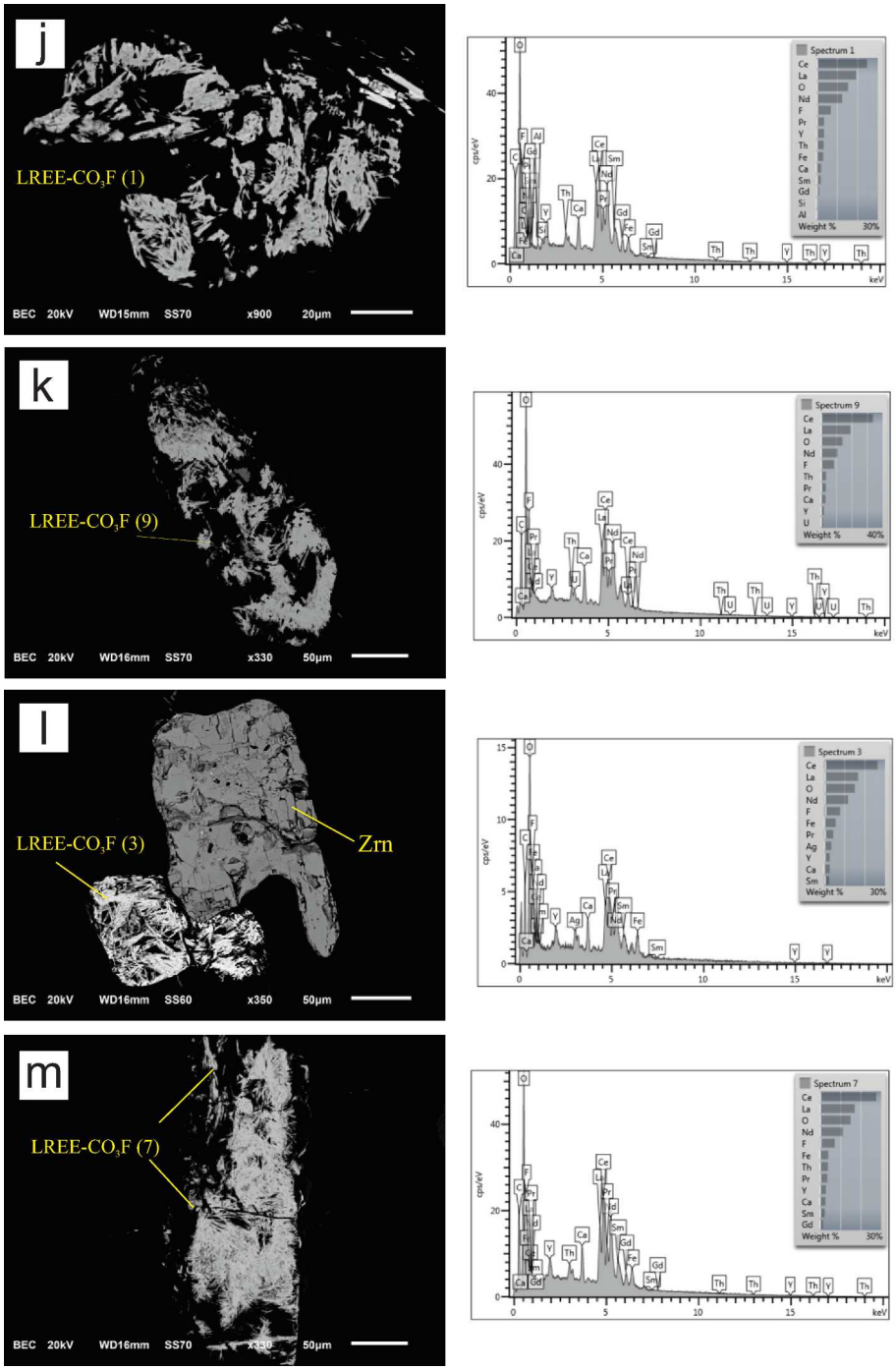

Fig. 6. (*continued*).

situ. Six samples were taken in intervals of approximately 50 cm, or at every notable changes of pedological horizons, in order to facilitate the understanding of the REE behaviour with depth and weathering degree. The outermost material was removed prior to sampling, to avoid material that has been directly exposed. The samples were taken at approximately 5–10 cm inwards the profile wall.

The uppermost horizon A is made up by an accumulation of decaying organic debris, loose dry leaves and roots along with loose quartz pebbles, silt and clay particles, in which plant roots develop. This horizon clearly changes to horizon B, dominated by red clays and quartz. This horizon is relatively homogeneous with brownish-red or brownish-orange hues; some prismatic structure can be seen. The horizon B gradually changes to C1, made up by orange saprolite, homogeneous or interlayered with whitish biotite-poor bands. At this point the granite's original texture and structure is still somewhat preserved. The redder areas are ascribed to the presence of Fe derived from biotite breakdown. This horizon gradually changes to horizon C2, made up by white saprolite, still clay-rich, but with it a rather friable texture. Downwards the profile the saprock of parental muscovite-biotite granite is *in situ*. All horizon boundaries are smooth. The local elevation is 636 m (measured with handheld GPS receiver).

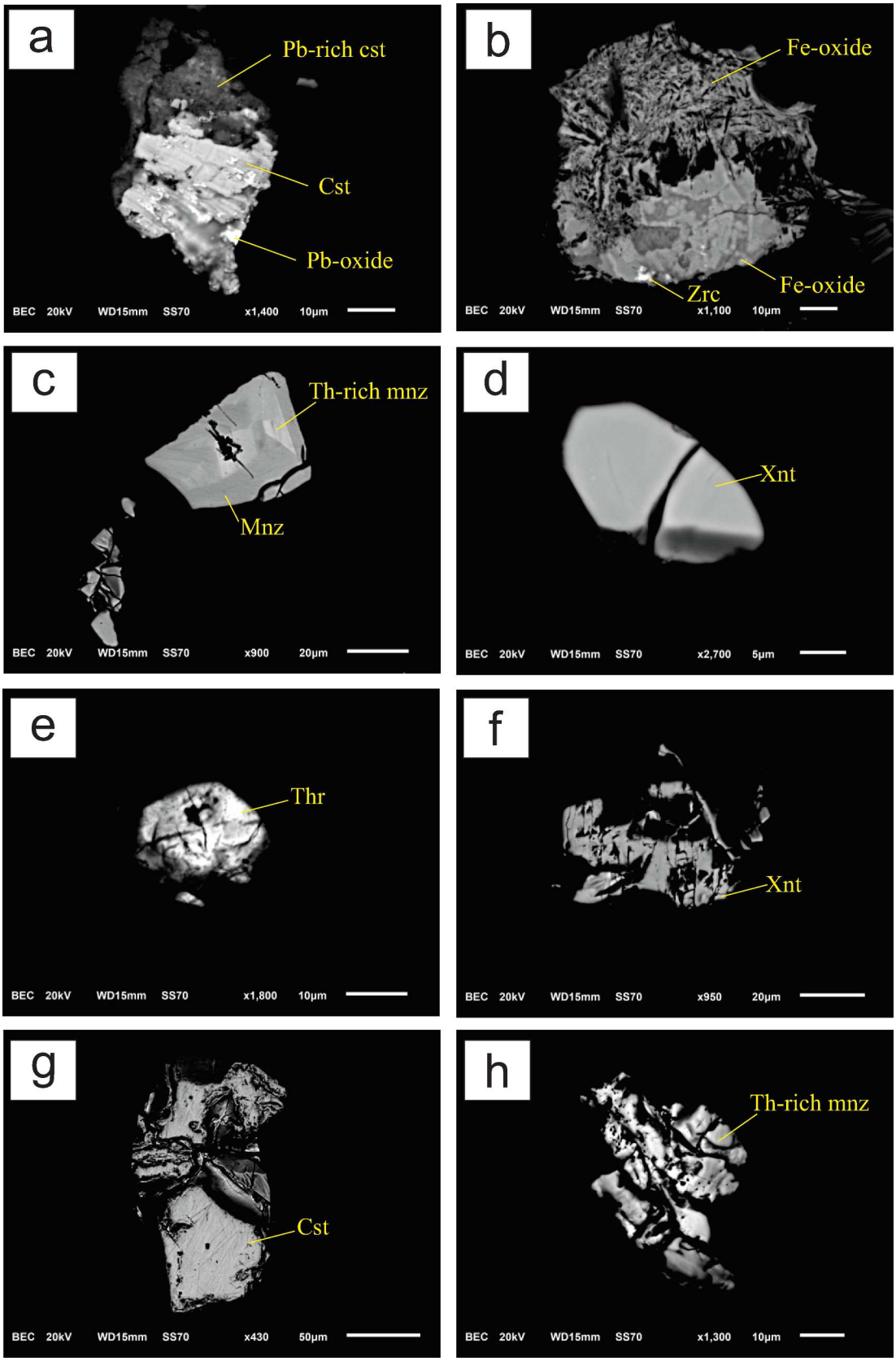

Fig. 7. SEM-BSE images of accessory minerals found in weathered samples. Mineral abbreviations from (Whitney and Evans, 2010).

6. Mineralogical characterization

6.1. XRD - bulk sample

Mineralogical characterization by means of XRD was carried out from saprock parental granite to top saprolite cover, samples 25–20. The diffractograms reveal the sequence of weathering starting with Na-feldspar breakdown in early stages, followed by kaolinite formation along with with the presence of micas and possibly illite. Kaolinite is more distinctively identified in sample 23, coincident with high REE contents. Sample 22 does not exhibit profound mineralogical changes, but has higher clay contents. Gibbsite firstly appears in sample 21 where kaolinite contents increase. Top sample 20 is marked by goethite appearance coexisting with the minerals aforementioned, in an horizon noticeable by SiO_2 removal, Al and Fe accumulation, relatively acidic pH ($\sim$ 4.5). Quartz is a common phase in all samples. The sequence of emergence of *kaolinite* > *illite* > *gibbsite* > *goethite* from bottom to top, follow a gradual acidification along the profile towards the top horizon, ranging from pH $\sim$ 5.5 in sample 24 to pH $\sim$ 4.5 in sample 20. The K-feldspar and Na-feldspar diffraction peaks do occur, but their exact end-member/composition were not defined by XRD. However, a thin section of sample 25 observed in petrographic microscope revealed microcline and orthoclase are somewhat more abundant than Na-feldspar. Beyond 32 °2 θ, minor quartz reflection peaks predominate in the diffractogram. The Fig. 4 exhibits the diffractograms of all samples.

6.2. XRD - clay-sized fraction

The clay-sized fraction of sample 20 was further analysed in detail, comparing the diffractograms of the air-dried oriented aggregate mount, further solvated with ethylene glycol and heated to 490 °C. Illite, kaolinite, gibbsite and goethite were the major phases identified (Fig. 5). Illite characteristic peaks have d-spacings of d(001) $\sim$ 10 Å, d(002) $\sim$ 4.95 Å and d(003) $\sim$ 3.33 Å. Kaolinite was identified by its relevant peaks at d(001) $\sim$ 7.1 Å and d(002) $\sim$ 3.56 Å, and gibbsite is marked by d(002) $\sim$ 4.83 Å. Goethite is indicated by a small peak at d(110) $\sim$ 4.13 Å. The air-dried and ethylene glycol solvated diffractograms are similar, but there is a visible change in the left shoulder of the first 001 illite peak, where a broad peak at d $\sim$ 11–12.5 Å is present. Combined, those peaks cover a broad interval $\sim 7 - 10°$ 2 θ, with highest intensity corresponding to d = 10.04 Å. After ethylene glycol solvation, the first illite peak remains in place, whereas the small peak on its left shoulder is slightly right-shifted and yields higher intensity readings, suggesting the presence of an interlayered swelling phase such as illite/smectite (I/S), or possibly illite/vermiculite (I/V). This peak is interpreted as part of a sequence of interlayered I/S and/or I/V, in which the main peak would be at d $\sim$ 24 Å ($\sim$ 4° 2 θ) not visible in the diffractogram 2 θ range, corresponding to the sum of illite d(001)$\sim$ 10 Å plus smectite or vermiculite at d $\sim$ 14 Å. Following the heat treatment, the 001 illite peak becomes much narrower and more intense, suggesting that another phase beyond illite - or interlayered with it - is contributing to the total intensities observed. The second and third reflections at d $\sim$ 5 and d $\sim$ 3.33 Å exhibit peaks with large, multi-peak tops, indicating the presence of more than one mica in addition to illite, such as biotite and/or muscovite. In fact, the saprolite is abundant in relict biotite and muscovite in the clay-sized fraction, the alteration of which could also yield to vermiculite. Halloysite-10 Å, if present, was not resolved from kaolinite due to difficulties in sample prepping and because it easily can dehydrates to halloysite-7 Å, which is very difficult to distinguish from kaolinite-7 Å.

6.2.1. SEM - REE minerals in parental granite

Three polished thin sections of sample 25 were submitted to scanning electron microscopy in order to generate SEM-BSE images and SEM-EDS spectra of REE minerals. The results indicate a selection of both LREE and HREE minerals, the former more abundant, which will be

Table 4
Results of sequential leaching.

		La	Ce	Pr	Nd	Sm	Eu	Gd	Tb	Dy	Ho	Er	Tm	Yb	Lu	(Y)	Extracted REY (ppm)	Whole-rock REY (ppm)	Residue (ppm)	Recovery (%)
20	step1	119.0	52.2	22.6	73.3	10.8	0.4	8.5	1.1	6.1	1.1	2.6	0.3	1.7	0.2	31.3	331.2			30.8
	step2	15.1	421.7	4.1	14.2	2.6	0.1	2.2	0.3	1.5	0.3	0.7	0.1	0.6	0.1	5.8	469.4			43.7
	total	134.1	473.9	26.7	87.5	13.4	0.5	10.7	1.4	7.6	1.4	3.3	0.4	2.3	0.3	37.1	800.6	1074.4	273.8	74.5
21	step1	62.8	18.6	12.2	39.0	5.5	0.2	4.2	0.5	2.9	0.5	1.3	0.2	0.8	0.1	15.0	163.8			28.1
	step2	18.3	289.6	3.9	12.8	2.1	0.1	1.7	0.2	1.0	0.2	0.4	0.1	0.3	0.03	3.9	334.4			57.3
	total	81.1	308.2	16.1	51.8	7.6	0.2	5.9	0.7	3.9	0.7	1.7	0.2	1.1	0.1	18.9	498.2	583.3	85.1	85.4
22	step1	77.9	16.7	14.9	47.2	6.5	0.2	4.7	0.6	3.2	0.5	1.3	0.2	0.8	0.1	16.1	190.9			29.5
	step2	29.6	228.3	6.4	19.7	3.1	0.1	2.0	0.3	1.3	0.2	0.5	0.1	0.3	0.04	4.6	296.5			45.8
	total	107.5	245.0	21.3	66.9	9.6	0.3	6.7	0.9	4.5	0.7	1.8	0.3	1.1	0.1	20.7	487.4	647.6	160.2	75.3
23	step1	68.9	24.0	12.9	40.3	5.8	0.2	4.2	0.6	2.9	0.5	1.1	0.1	0.7	0.1	15.0	177.3			16.5
	step2	76.5	446.4	12.9	39.7	6.5	0.2	4.3	0.5	2.6	0.4	0.8	0.1	0.5	0.1	9.8	601.3			55.9
	total	145.4	470.4	25.8	80.0	12.3	0.4	8.5	1.1	5.5	0.9	1.9	0.2	1.2	0.2	24.8	778.6	1075.2	296.6	72.4
24	step1	89.3	24.6	17.6	58.3	9.1	0.3	7.2	1.0	4.9	0.8	2.0	0.2	1.3	0.2	25.2	242.0			28.3
	step2	73.2	298.2	12.0	39.1	6.6	0.2	5.1	0.7	3.2	0.5	1.0	0.1	0.7	0.1	12.9	453.6			53.0
	total	162.5	322.8	29.6	97.4	15.7	0.5	12.3	1.7	8.1	1.3	3.0	0.3	2.0	0.3	38.1	695.6	855.3	159.7	81.3
25	step1	27.5	24.4	4.6	16.5	3.0	0.1	4.0	0.7	4.3	0.9	2.7	0.4	2.1	0.3	38.6	130.1			15.7
	step2	108.2	144.4	15.4	51.7	8.8	0.2	7.4	1.0	4.8	0.8	1.8	0.2	1.3	0.2	30.2	376.4			45.4
	total	135.7	168.8	20.0	68.2	11.8	0.3	11.4	1.7	9.1	1.7	4.5	0.6	3.4	0.5	68.8	506.5	828.2	321.7	61.2

Residue = Whole-rock REE - total extracted.
Recovery = (Total extracted / whole-rock REE)x100.

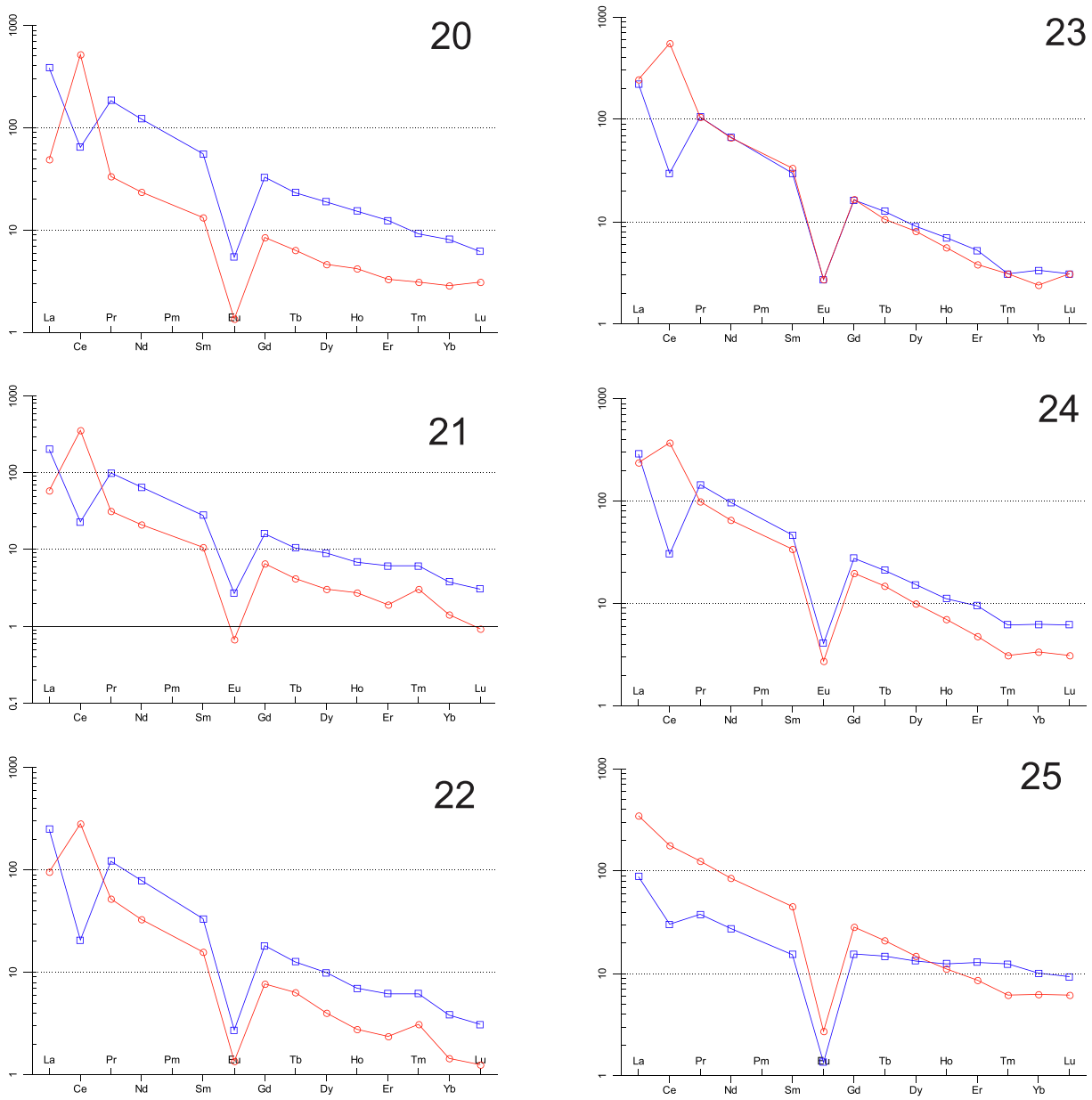

Fig. 8. Chondrite-normalized patterns of extracted REE after the complete leaching process. Step 1 - blue line; Step 2 - red line. Chondrite values from (Boynton, 1984).

detailed below.

6.2.1.1. REE silicate and phosphates. Monazite-(Ce), xenotime-(Y) and zircon are the ordinary representatives of phosphate and silicate mineral groups. They commonly occur included in biotite, but are also found in the quartz-feldspathic matrix, although rare. Monazite of the studied sample is Ce-selective, followed by La, Nd, Pr and Sm in this order of abundance, with Y and Gd as the HREE representatives; Th is notably detected in the SEM-EDS spectra as well (Fig. 6a). Xenotime is highly Y-selective, with minor Dy, Er, Yb and Gd amounts. No compositional zonation was observed in phosphates, but zircon is highly heterogeneous and metamictic. These minerals are commonly associated, as illustrated in Fig. 6b. Zr and Th-phases are commonly found in the vicinity of other REE-phases, associated or somehow related. Zircon is highly metamict, euhedral to subhedral, pronounced "brecciated" texture with minute rounded inclusions where U and Th are concentrated. Dark stripes within zircon were observed, possibly following preferable crystallographic directions. SEM-EDS spectra of those stripes is akin to that of an ordinary zircon; the only difference is that Ca and Fe are detected in trace amounts (Fig. 6d). Thorite was found as zircon inclusions (Fig. 6e) and as a rounded 200μ m grain. SEM-EDS spectra on homogeneous areas of the latter, has yielded minor amounts of Y and Nd, in addition to Fe and F, whereas the dark spots within the grain are areas where Y contents are notably higher (Fig. 6f).

6.2.1.2. LREE fluorocarbonates. The majority of REE-phases in sample 25 are represented by LREE fluorocarbonates. They were determined by comparing the intensity of C-peaks yielded by their SEM-EDS spectra with those of minerals such as zircon and quartz. In the two latter, the C-peak is approximately, or less than approximately, 10 cps/eV, mainly derived from the carbon-coating, so that value was used as reference number to indicate non-carbonate minerals. The SEM-EDS spectra of LREE fluorocarbonates yields C-peaks with twice that intensity, at 20–24 cps/eV, suggesting the existence of C beyond the coatings. They commonly occur as pseudomorph needle-like grains, as radiating fibers intersecting each other forming clusters with voids in between,

suggesting volume reduction upon a previous phase (Fig. 6e-m). Dimensions vary, but the average is around 100μ m. They are strongly LREE-selective, dominated by Ce, La, Nd and Pr, in this order of abundance, plus Y, Th, Ca and Fe in variable minor amounts. They occur isolated, included in biotite, or associated with zircon, monazite-(Ce) and thorite. Furthermore, LREE fluorocarbonate needles were found growing upon fluorite (Fig. 6h).

6.3. SEM - REE minerals in weathered granite

Samples 23, 21 and 20 were mounted in resin blocks and analysed in SEM, in order to verify the accessory minerals in weathered samples. Monazite-(Ce), Th-rich monazite, xenotime-(Y), thorite, Ti-bearing Fe oxide, cassiterite, Pb-rich cassiterite, Pb-oxide and zircon were the minerals found (Fig. 7a-h). The REE fluorocarbonates found in parental granite were not detected in weathered samples, at least in the analysed resin blocks, suggesting that they did not withstand the weathering degree at this point. Some REE fluorocarbonate can still exist, but it is feasible to believe that most of it have been dissolved into REE ions that were either leached out, adsorbed on clays and/or incorporated into secondary phases, forming the overall REE grade in weathered samples.

7. Results of sequential leaching

The sequential extraction was carried out in 1 g of bulk powder sample in order to assess the amount of recoverable REE, the results summarized in (Table 4). The recovery rate was found to be high, up to 85% of recovered REE relative to whole rock REE contents, but this is mainly attributable to Ce. The highest REE recovery rate was yielded by sample 21, from which 498 out of 583 ppm were extracted. However, in absolute numbers, sample 23 yielded higher values, where 779 ppm out of 1,075 ppm was recovered. All samples after the complete extraction procedure yielded descendent REE patterns, reproducing the granite's LREE affinity and indicating the lower solubility of the HREE in the chemicals used. Fig. 8 illustrates the chondrite-normalized REE patterns after each extraction. The inversion of Ce anomaly between steps draws the attention: negative Ce anomaly predominates in the REE pattern obtained after step-1, in opposition to the mostly positive Ce anomaly following step-2. A particular case is worth mentioning: in sample 21, the sum of extracted Ce after all steps totalized 308 ppm, whereas Ce quantified in whole rock analysis yielded 303 ppm, which gives about 5 ppm extracted in excess. We believe this is a matter of interlabs accuracy (the quantification of extracted REE and whole rock analysis were carried out in different labs) and due to natural sample aliquots variation - one aliquot sent to whole rock analysis and the other to leaching experiment.

Overall, step-1 extraction yielded higher REE contents, except for Ce, which is better recovered by step-2. The contribution of step-1 progressively decreases downwards the profile until sample 25, where the pattern is inverted and it contributes less with the total extracted. The proportion of extracted REE after step-1 (exchangeable REE) in relation to whole-rock REE ranges from 16 to 31%. This is a relatively small proportion compared with the Serra Verde IAD and with other ores reacted with ammonium sulphate (Sanematsu and Kon, 2013; Sanematsu et al., 2013; Ward, 2017; Estrade et al., 2019). Step-2 yielded REE contents of 297 up to 601 ppm but, Ce alone, on average, corresponds to 80% of that fraction, indicating that this element is preferentially associated with oxides or was recovered from phases with higher solubility in reducing conditions (hydroxylammonium chloride is a reducing agent). Whole rock analysis indicate that Ce is concentrated in uppermost sample 20 and in the middle of the profile at sample 23, which is coincident with the higher Ce recovered by the leaching reactions. The REE recovery rate is also higher following step-2 when compared with step-1. On average, the recovery rate following step-2 is 50% higher than step-1. The chondrite-normalized REE patterns produced after step-2 are marked by strong positive Ce anomalies, negative Eu anomalies, and descendent fractionation towards the HREE.

Table 5
Calculated Tau coefficients of elements along the weathering profile, with Al as the immobile element.

Sample	20	21	22	23	24
SiO_2	−0.65	−0.27	−0.20	−0.14	−0.11
Fe_2O_3	0.34	−0.02	0.05	0.03	0.23
CaO	−0.99	−0.98	−0.98	−0.95	−0.96
MgO	−0.65	−0.85	−0.79	−0.65	0.13
Na_2O	−0.97	−0.92	−0.91	−0.89	−0.85
K_2O	−0.73	−0.35	−0.22	−0.05	0.07
TiO_2	0.33	−0.02	0.07	0.25	0.25
Nb	0.19	−0.03	0.08	0.16	0.04
Th	0.06	0.08	0.09	−0.06	0.27
Sn	1.14	−0.30	−0.28	−0.33	0.38
Zr	−0.24	−0.21	−0.22	−0.04	−0.08
LREE	−0.33	−0.43	−0.31	0.30	0.02
HREE	−0.62	−0.57	−0.48	−0.51	−0.42

The residue, listed in the same Table 4, means the fraction of REE that were not recovered after all steps, probably because they were unaffected by the chemicals used in the process. REE contents remained in the residue ranges from 85 to 322 ppm, the latter in sample 25 - saprock - possibly due to its lower weathering degree.

8. Mass transfer and volumetric strain

The compositional change from saprock to topsoil was quantified in order to assess the elements enrichment/depletion along the profile, comparing the element contents of the weathered samples with those of sample 25 (parental muscovite-biotite granite). The fractional mass change "Tau" ***(τ)*** between samples was calculated by comparing the content (**C**) of an element ***(j)*** in a weathered sample ***(w)*** with the content of the same element in the parental material ***(p)***, both normalized to an immobile element ***(i)***, according to the equation presented by (Brimhall and Dietrich, 1987):

$$\tau_{j,w} = \frac{C_{i,p}C_{j,w}}{C_{i,w}C_{j,p}} - 1, \quad (1)$$

where $-1 \leq \tau_{ij} < 0$ indicates element depletion, $0 < \tau_{ij} < \infty$ indicates element enrichment and $\tau = 0$ means no mass transfer. Some elements commonly regarded as conservative during granite weathering such as Th, Sn, Ti, Hf, Zr, Fe, Nb and Al were considered as immobile candidates. Zr, Th and Hf were disregarded because they are mostly hosted in zircon, which can be highly heterogeneously distributed in granitic rocks. In addition to it, the zircon grains observed in this study are highly metamictic and fractured, which could facilitate for those elements to "escape" zircon and be somehow mobilized in the weathering profile. Sn is mainly incorporated in cassiterite - found in the most weathered sample - but it is also heterogeneously distributed in the SDG: the Pela Ema mine and its vicinity is only a locally enriched cassiterite area, and do not represent the overall granite. Fe was not used as immobile element because it is very sensitive to redox conditions. Ti - at least in samples of this study - is mostly incorporated in Fe-oxides and was not found forming a phase of its own, although detrital ilmenite had been found in other areas of the massif (Santana et al., 2015). This is suggestive that Ti-phases are not homogeneously distributed in the SDG. Nb is concentrated in trace amounts, was not identified forming a phase in samples analysed in this study, but is known to occur in the Serra Verde deposit area (Ward, 2017), indicating irregular distribution. In opposition to the elements aforementioned, Al_2O_3 as a major constituent is rather homogeneous and inert during chemical weathering, and therefore was chosen as immobile element. The obtained τ coefficients are summarized in Table 5 and discussed in the relevant section.

The numbers reveal that the oxides of Si, Ca, Mg, Na and K were strongly removed during the weathering process. The depletion of Si is progressive upwards, with τ values, from sample 24 to 20, ranging from

−0.11 to −0.65. Depletion of alkalis start in the early stages of weathering, being almost completely removed in the uppermost horizon; Nb, Th and Zr are relatively conservative. Tin is an exception, being strongly gained in the uppermost horizon, likely due to cassiterite residual concentration. The weathering also promoted gain of Fe and Ti in sample 20 horizon with $\tau = 0.34$ and 0.33, respectively, explained by the accumulation of Fe-oxides and biotite relict. The LREE are mainly concentrated in sample 23, whereas the HREE are depleted along the whole profile.

The volumetric strain (ϵ) was quantified based in the equation presented by (Brimhall and Dietrich, 1987), assuming Al as the immobile element, as follows:

$$\epsilon_{i,w} = \frac{\rho_p C_{i,p}}{\rho_w C_{i,w}} - 1, \quad (2)$$

where the greek letter ρ denotes for dry bulk density and the other subscripts as already explained in Eq. (1). Average density values for sample 25, the saprolite (samples 24–21) and for the uppermost soil sample 20 were taken from (Ward, 2017) (p. 208): 2.5, 1.71 and 1.56 g/cm3, respectively. The ϵ values obtained for samples 20 to 24 are −0.25, 0.12, 0.22, 0.27 and 0.31, respectively. Since $\epsilon > 0$ indicates volume dilation and $\epsilon < 0$ indicates volume collapse, there was progressive volume increase from sample 24 to 21, and volume reduction in the uppermost horizon, relative to the parental granite (sample 25).

9. Discussions

The presence of LREE fluorocarbonates is suggestive of CO,F-rich fluids during the granite evolution. These phases are even more abundant than monazite and xenotime in the parental granite, and since they are more easily dissolved during weathering (Sanematsu and Watanabe, 2016) they play a major role in supplying the REE to the weathered system. The characteristics of the LREE fluorocarbonates such as texture, dimension and mode of occurrence suggest secondary or hydrothermal processes, upon primary minerals. In most cases, the LREE fluorocarbonates needles/rosettes occur as pseudomorphs after euhedral precursors, often filling vesicles. Indirect evidence of their secondary nature is the occurrence of a thorite core surrounded by a rim of LREE fluorocarbonates, as well as the intergrowth of fluorite and LREE fluorocarbonates (Fig. 6f,h), which could be explained in accordance to the equations presented by (Littlejohn, 1981):

$$Allanite + F, CO_2, H_2O \rightarrow Thorite + Bastnäsite + Montmorillonite + Ca^{2+} \quad (3)$$

$$Allanite + CO_2, F \rightarrow Fluorite + Synchysite + Chamosite \quad (4)$$

The reactions require allanite as a precursor phase, but allanite was not detected in the polished sections of saprock muscovite-biotite granite (sample 25). The allanite absence could be due the low representativeness that a 4x2 cm thin section provides of a batholith-sized massif - if it still occurs in the parental rock or as relicts in the weathered samples - or an evidence that most of it was altered and replaced with secondary phases. (Macambira, 1983; Teixeira and Botelho, 2006; Santana et al., 2015; Ward, 2017) report allanite in the SDG corroborating its existence in the massif - but is more common in the biotite granite than in the muscovite-biotite granite facies. The Mocambo granitic massif studied by (Vieira et al., 2019) and the Pedra Branca granitic massif surveyed by (Costa et al., 2020) are granites related to the SDG that also belong to the Goiás Tin Province. In those, the authors also found allanite, in addition to other REE-bearing minerals. Titanite is another potential precursor phase for the LREE fluorocarbonates (Pan et al., 1993; Price et al., 1999; Middleton et al., 2013), and is a common accessory in the SDG, being reported by (Macambira, 1983; Bilal et al., 1997; Teixeira and Botelho, 2006; Ward, 2017). Titanite was found in heavy mineral concentrates reported by (Santana et al., 2015), corroborating its existence in the SDG.

The τ values and absolute REE contents yield a trend of enrichment/depletion in specific horizons along the transect. La, Pr and Nd are clearly being concentrated in sample 23; likewise is Ce, but in higher degree than the others, specially in sample 23 horizon and in the uppermost horizon. Consequently, the REE budget in leachate solutions are mostly composed by Ce, which was better recovered following step-2. As mentioned, that step was carried out with hydroxylammonium chloride - a reducing agent - suggesting that Ce is more related to phases that have higher solubility under reducing conditions. Unlike other studies such as those reviewed by (Sanematsu and Watanabe, 2016), the accumulation of Ce occurs in two horizons: the uppermost one and in sample 23 horizon. The former is marked by positive Ce anomalies which, according to (Brookins, 1988) is a response to the near-surface Ce^{3+} oxidation to Ce^{4+} into cerianite at ambient conditions. However, no cerianite was found in saprock or weathered samples herein analysed. One possible explanation is that there is cerianite indeed, but the low representativeness of the resin blocks constrains the search for the mineral. A second possible explanation is that most Ce in this specific weathered system is not Ce^{4+}, but Ce^{3+} and incorporated, or somehow associated, to Fe-oxides without further precipitation into cerianite. Studies have shown that Ce is not necessarily oxidised and strongly fractionated from other REE during weathering (Janots et al., 2015), and samples samples with negative Ce anomalies can still contain significant amounts of Ce^{4+}(Ram et al., 2019). In any case, regarding the presence of Ce as either Ce^{4+} and/or Ce^{3+}, it is clearly being concentrated in the uppermost horizons, illuviated from mid-profile to accumulate in sample 23 horizon, and predominately recovered using a reducing agent (step-2).

The other LREE exhibits illuviation from upper horizons and concentration in sample 23 horizon, mostly as weakly adsorbed species because they were mostly recovered following step-1. In this respect, the material analysed can be considered an ion adsorption-type (except Ce), even though the REE contents in leachate solutions are lower than those from other IAD occurrences (Sanematsu and Kon, 2013; Sanematsu et al., 2013; Ward, 2017; Estrade et al., 2019). The HREE are all depleted in overlying horizons above the parental granite. In fact, the parental granite is relatively poor in HREE minerals of their own and this reflects in the overall HREE contents in weathered material. Other HREE, specially Y, are incorporated in LREE-fluorocarbonates as impurities possibly derived from thorite and/or zircon during hydrothermal mobilization, so these minerals are ascribed to contribute to the overall HREE, even in low quantitites. In addition to it, the minerals in which the HREE are incorporated, zircon and xenotime, are more resistant to weathering then the LREE fluorocarbonates, reflecting in lower availability of HREE to be adsorbed on clays. Secondarily, the HREE depletion during granite weathering can be explained in terms of their higher stability with ligands that might be present in percolating water, under supergene conditions. Studies report that the HREE are more stable with OH^- and CO32– complexants, and therefore more susceptible to be leached out from the profile (Klungness and Byrne, 2000; Luo and Byrne, 2004; Aide, 2012). Fluorine released from the breakdown of LREE fluorocarbonates could also contribute to leach out the HREE, as they form a more stable complex than the LREE (Millero, 1992; Gramaccioli et al., 1999). The role of organic acids is still controversial in terms of which REE form the most stable complexes, but they could also play a role in mobilizing the HREE out of the weathering system.

The volumetric strain parameters indicate dilation of the initial rock volume in horizons of samples 24 to 21 ($\epsilon > 0$) and volume collapse in upper horizon sample 20 ($\epsilon < 0$). The physical changes in this case are best explained in terms of mass gain/loss coupled with changes in porosity. Sample 20 horizon contraction ($\epsilon < 0$) can be explained in terms of the intense mass loss with percolating water, specially of SiO_2, K_2O and Na_2O, which exceeds the effects of volume gain from clays and residual enrichment of Al_2O_3, and dense Fe-oxides, Zr, Ti, Sn and Nb-phases. All the lower horizons exhibit volume dilation, explained by

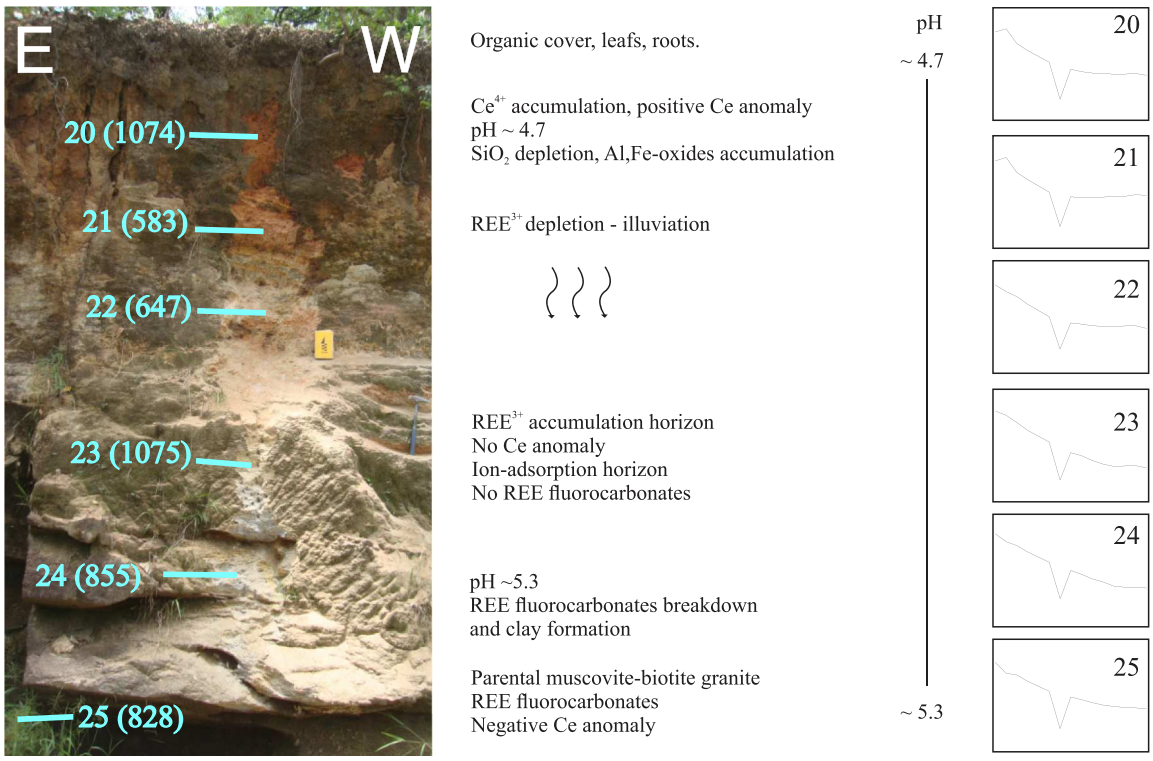

Fig. 9. Schematic model of REE mobility in the weathering profile surveyed.

the increase in porosity with weathering and lower ratios of mass loss than the uppermost horizon. In addition to it, the weathering of micas can cause volume expansion and physical disturbance of minerals in the vicinity, increasing the overall porosity (Goodfellow et al., 2016; Hayes et al., 2019).

The kinetics of REE mobility during pedogenetic processes seems to be a balance between many physico-chemical factors as reviewed by (Laveuf and Cornu, 2009), but in this study we discuss this matter in three fronts, all influencing on its own way: clay amount and weathering degree; clay type and its cation exchange capacity (CEC); and point of zero charge (PZC). The correlation of clay amount and weathering degree with REE content is straightforward, i.e., the more weathered the parental granite is the more argillaceous it becames. As natural REE reservoirs, the clay-rich horizons tend to be potentially more REE enriched. One example is sample 25 (clay-poor), where Step-1 contribution to REE recovery is minimum compared with other clay-rich samples where the same step is more significant. The CEC of clay minerals found in this study increases in the order *kaolinite* < *illite* < *vermiculite* < *smectite* (Lepsch, 2016), but since the last two are minor constituents, the first two actually dictate the REE accumulation (except for Ce) in the weathered profile of the ion-exchangeable fraction. Both illite and kaolinite are identified in early stages of weathering, corroborating their importance in retaining the REE. Other phases such as gibbsite and goethite only appear in top samples 21 and 20, where drainage is higher and pH is more acidic. In the uppermost horizon, acidic pH, excess of Al_2O_3 and organic acids constrain the adsorption capacity of clays because more H^+ and Al^{3+} are available to neutralize the clay's negative surface charge, which otherwise could be occupied by a REE^{3+} ion, but is counterbalanced by the clay abundance and Fe, Mn-oxides (preferential hosts for Ce). The point of zero charge (PZC) of kaolinite and illite is 3.6 and 2.5 respectively (Kosmulski, 2009) and, as the pH of the weathered profile is above that, ranging from ~ 4.5–5.5, both kaolinite and illite are negatively charged surfaces and liable of receiving the REE as adsorbed species in all horizons. The accumulation horizon where sample 23 is located could reflect the highest adsorption capacity of the REE species on clays at a less acidic pH ~ 5.3, coupled with the highest rate of REE fluorocarbonates breakdown. The Fig. 9 summarizes the REE mobility model along the profile in respect to the general features discussed.

10. Conclusions

The overall features observed in the weathering profite enable it to be compared with other important granite-related REE mineralizations. The studied transect exhibits REE enrichment when compared with the parental granite, but the weakly adsorbed REE (the ion-exchangeable fraction), is somewhat lower than other deposits worldwide. Kaolinite and illite are the major clays, acting as depository for the adsorbed REE ions. The leaching experiments proved to be specially suitable for the recovery of Ce, specially following step-2, associated with Fe-oxides. SEM analysis attested the existence of REE fluorocarbonates as the main REE supliers during the granite weathering. Two levels of the profile were found to concentrate the REE: the uppermost horizon, dominated by Ce and the mid-profile sample 23 horizon, regarded as the accumulation zone for the illuviated REE from horizons above. Compared with the coarse-grained biotite granite from Serra Verde deposit, the fine-grained muscovite-biotite granite herein analysed yields lower REE grade and overall REE recovery. However, the study is useful to enhance the understanding of the REE ion adsorption in the SDG. Given its batholith dimensions and multiple facies, more research in other facies within the massif could build up to its overall characterization.

Declaration of Competing Interest

The authors declare that they have no known competing financial interests or personal relationships that could have appeared to influence the work reported in this paper.

Acknowledgements

This study was financed in part by the Coordenação de

Aperfeiçoamento de Pessoal de Nível Superior - Brasil (CAPES) - Finance Code 001. SEM analysis were carried out in the Microanalysis and Microscopy lab - DEGEO/EM - Universidade Federal de Ouro Preto, Minas Gerais, Brazil.

References

Barbosa, O., Batista, M., Dyer, R., Braun, O. Cotta, J., 1969 Projeto brasília–goiás: geologia e inventário dos recursos minerais, Goiânia: DNPM.

Marini, O.J., Fuck, R.A., Dardenne, M.A., De Faria, Á., 1977. Contribuição à geologia do pré-cambriano da porção central de Goiás. Revista Brasileira de Geociências 7 (4), 304–324.

Marini, O., Botelho, N., 1986. A província de granitos estaníferos de Goiás. Braz. J. Geol. 16 (1), 119–131.

Macambira, M.J.B., 1983. Ambiente geológico e mineralizações associadas ao granito Serra Dourada (extremidade meridional)-Goiás. University of Pará. Master's thesis.

Marini, O.J., Botelho, N.F., Rossi, P., 1992. Elementos terra raras em granitóides da província estanífera de Goiás. Braz. J. Geol. 22 (2), 61–72.

Bilal, E., Moutte, J., Botelho, N., Marini, O., Andrade, G., 1997. Geochemistry of two proterozoic A-type granites of Goiás State, Brazil: possible links with rapakivi series. Ann. Brazilian Acad. Sci. 69, 349–365.

Teixeira, L.M., Botelho, N.F., 2006. Comportamento geoquímico de ETR durante evolução magmática e alteração hidrotermal de granitos: exemplos da província estanífera de Goiás. Braz. J. Geol. 36 (4), 679–691.

Radambrasil, P. Folha SD. 22 Goiás, 1981. Geologia, geomorfologia, pedologia, vegetacao, uso potencial da terra. Rio de Janeiro: Ministério das Minas e Energia, Departamento Nacional de Fundução Mineral, Rio de Janeiro, Brasil.

Marini, O. J., Barbosa, G. V., Dardenne, M.4., Faria, A. C., Fuck, A. 1974 a - Projeto Serra Dourada, relatório final-geociências. 187 p, Brasília, FUB/Dept.

Santana, V., 2013. Mineralogical and geochemical characterization of rare earth element occurences in the Serra Dourada granite, Goiás/Tocantins, Brazil, Master's thesis. University of Brasília.

Sanematsu, K., Watanabe, Y., 2016. Characteristics and genesis of ion-adsorption type deposits. Reviews in Economic Geology.

Santana, I.V., Wall, F., Botelho, N.F., 2015. Occurrence and behavior of monazite-(Ce) and xenotime-(Y) in detrital and saprolitic environments related to the Serra Dourada granite, Goiás/Tocantins States, Brazil: Potential for REE deposits. J. Geochem. Explor. 155, 1–13.

Ward, P. Carmen, Controls on the enrichment of the Serra Verde rare earth deposit, Brazil, Ph.D. thesis, Imperial College London (2017).

Chi, R., Tian, J. Weathered crust elution-deposited rare earth ores, Nova Science Publishers, Inc., 2008.

Bao, Z., Zhao, Z., 2008. Geochemistry of mineralization with exchangeable REY in the weathering crusts of granitic rocks in South China. Ore Geol. Rev. 33 (3-4), 519–535.

Brookins, D.G., 1988. Eh-pH Diagrams for Geochemistry. Springer-Verlag, New York, p. 176.

Sanematsu, K., Kon, Y., Imai, A., Watanabe, K., Watanabe, Y., 2013. Geochemical and mineralogical characteristics of ion-adsorption type REE mineralization in Phuket. Thailand, Mineralium Deposita 48 (4), 437–451.

Marques, G.C., 2009. Geologia dos grupos Araí e Serra da Mesa e seu embasamento no sul do Tocantins. Universidade de Brasília, Brasília (MSc Dissertation, p. 120p.sa e seu embasamento no sul do Tocantins. Universidade de Brasília, Brasília (MSc Dissertation, p. 120p.

Mentani, T., Ohmura, T., Watanabe, Y., Urabe, T., 2010. So-called ion-adsorption type REE deposits found in weathered crust of ilmenite-series granite in northern Vietnam. 2010 GSA Denver Annual Meeting. GSA.

Sanematsu, K., Murakami, H., Watanabe, Y., Duangsurigna, S., Siphandone, V., 2009. Enrichment of rare earth elements (REE) in granitic rocks and their weathered crusts in central and southern Laos. Bulletin of the Geological Survey of Japan 60 (11–12), 527–558. https://doi.org/10.9795/bullgsj.60.527.

Padrones, J.T., Imai, A., Takahashi, R., 2017. Geochemical behavior of rare earth elements in weathered granitic rocks in northern Palawan, Philippines. Resour. Geol. 67 (3), 231–253.

Estrade, G., Marquis, E., Smith, M., Goodenough, K., Nason, P., 2019. REE concentration processes in ion adsorption deposits: Evidence from the Ambohimirahavavy alkaline complex in Madagascar. Ore Geol. Rev. 112, 103027.

Ure, A., Quevauviller, P., Muntau, H., Griepink, B., 1993. Speciation of heavy metals in soils and sediments. An account of the improvement and harmonization of extraction techniques undertaken under the auspices of the BCR of the commission of the european communities. International journal of environmental analytical chemistry 51 (1–4), 135–151.

Thomas, R.P., Ure, A.M., Davidson, C.M., Littlejohn, D., Rauret, G., Rubio, R., López-Sánchez, J.F., 1994. Three-stage sequential extraction procedure for the determination of metals in river sediments. Anal. Chim. Acta 286 (3), 423–429.

Rauret, G., López-Sánchez, J., Sahuquillo, A., Rubio, R., Davidson, C., Ure, A., Quevauviller, P., 1999. Improvement of the BCR three step sequential extraction procedure prior to the certification of new sediment and soil reference materials. J. Environ. Monit. 1 (1), 57–61.

Marini, O., Fuck, R., Danni, J., Dardenne, M., Loguercio, S., Ramalho, R., 1984. As faixas de dobramentos Brasília, Uruaçu e Paraguai-Araguaia eo maciço mediano de Goiás. Geologia do Brasil 251–303.

de Brito Neves, B.B., M. d. C. Campos Neto, R. A. Fuck,, 1999. From rodinia to western gondwana: an approach to the brasiliano-pan african cycle and orogenic collage. Episodes 22, 155–166.

Dardenne, M.A., 2000. In: Dardenne, M., Cordani, U., Milani, E., Thomaz Filho, A., Campos, D. (Eds.), Tectonic Evolution of South America, 1. CPRM, Rio de Janeiro.

Valeriano, C.M., Pimentel, M.M., Heilbron, M., Almeida, J.C.H., Trouw, R.A.J., 2008. Tectonic evolution of the Brasília belt, central Brazil, and early assembly of gondwana. Geological Society, London, Special Publications 294 (1), 197–210.

Pimentel, M.M., Heaman, L., Fuck, R.A., Marini, O.J., 1991. U-Pb zircon geochronology of precambrian tin-bearing continental-type acid magmatism in central Brazil. Precambr. Res. 52 (3–4), 321–335.

Teixeira, L.M., 2002. Caracterização de minerais portadores de terras raras e sua aplicação à petrologia e geocronologia de granitos das subprovíncias Tocantins e Paranã - Goiás. University of Brasília. Ph.D. thesis.

Shand, S.J., 1943. Eruptive rocks: their genesis, composition, classification, and their relation to ore deposits with a chaper on meteorites. Tech. rep.

Sanematsu, K., Kon, Y., 2013. Geochemical characteristics determined by multiple extraction from ion-adsorption type REE ores in Dingnan county of Jiangxi province, south China. Bulletin of the Geological Survey of Japan 64 (11–12), 313–330.

Brimhall, G.H., Dietrich, W.E., 1987. Constitutive mass balance relations between chemical composition, volume, density, porosity, and strain in metasomatic hydrochemical systems: results on weathering and pedogenesis. Geochim. Cosmochim. Acta 51 (3), 567–587.

Littlejohn, A., 1981. Alteration products of accessory allanite in radioactive granites from the canadian shield. Tech. rep.

Vieira, C.C., Botelho, N.F., Garnier, J., 2019. Geochemical and mineralogical characteristics of reey occurrences in the Mocambo granitic massif tin-bearing A-type granite, central Brazil, and its potential for ion-adsorption-type REEY mineralization. Ore Geol. Rev. 105, 467–486.

Costa, N., Botelho, N., Garnier, J., 2020. Concentration of rare earth elements in the Faixa Placha tin deposit, Pedra Branca A-type granitic massif, central Brazil, and its potential for ion-adsorption-type REEY mineralization. Ore Geol. Rev. 123, 103606.

Pan, Y., Fleet, M.E., MacRae, N.D., 1993. Late alteration in titanite (CaTiSiO5): redistribution and remobilization of rare earth elements and implications for U/Pb and Th/Pb geochronology and nuclear waste disposal. Geochim. Cosmochim. Acta 57 (2), 355–367.

Polo, H.J.d.O., Diener, F.S., 2017. Folha sd. 22-xd-ii Mata Azul. carta geológica-escala 1, 100.000.

Price, J.D., Hogan, J.P., Gilbert, M.C., London, D., Morgan, G.B., 1999. Experimental study of titanite-fluorite equilibria in the A-type Mount Scott granite: Implications for assessing F contents of felsic magma. Geology 27 (10), 951–954.

Middleton, A.W., Förster, H.-J., Uysal, I.T., Golding, S.D., Rhede, D., 2013. Accessory phases from the Soultz monzogranite, Soultz-Sous-Forêts, France: implications for titanite destabilisation and differential REE, Y and Th mobility in hydrothermal systems. Chem. Geol. 335, 105–117.

Janots, E., Bernier, F., Brunet, F., Muñoz, M., Trcera, N., Berger, A., Lanson, M., 2015. Ce (iii) and Ce (iv)(re) distribution and fractionation in a laterite profile from Madagascar: insights from in situ xanes spectroscopy at the Ce liii-edge. Geochim. Cosmochim. Acta 153, 134–148.

Ram, R., Becker, M., Brugger, J., Etschmann, B., Burcher-Jones, C., Howard, D., Kooyman, P.J., Petersen, J., 2019. Characterisation of a rare earth element- and zirconium-bearing ion-adsorption clay deposit in Madagascar. Chem. Geol. 522, 93–107.

Klungness, G.D., Byrne, R.H., 2000. Comparative hydrolysis behavior of the rare earths and yttrium: the influence of temperature and ionic strength. Polyhedron 19 (1), 99–107.

Luo, Y.-R., Byrne, R.H., 2004. Carbonate complexation of yttrium and the rare earth elements in natural waters. Geochim. Cosmochim. Acta 68 (4), 691–699.

Aide, M.T., C., 2012. Aide, Rare earth elements: their importance in understanding soil genesis, ISRN. Soil Sci.

Millero, F.J., 1992. Stability constants for the formation of rare earth-inorganic complexes as a function of ionic strength. Geochim. Cosmochim. Acta 56 (8), 3123–3132.

Gramaccioli, C.M., Diella, V., Demartin, F., 1999. The role of fluoride complexes in REE geochemistry and the importance of 4f electrons; some examples in minerals. Eur. J. Mineral. 11 (6), 983–992.

Goodfellow, B.W., Hilley, G.E., Webb, S.M., Sklar, L.S., Moon, S., Olson, C.A., 2016. The chemical, mechanical, and hydrological evolution of weathering granitoid. J. Geophys. Res. Earth Surf. 121 (8), 1410–1435.

Hayes, J.L., Riebe, C.S., Holbrook, W.S., Flinchum, B.A., Hartsough, P.C., 2019. Porosity production in weathered rock: Where volumetric strain dominates over chemical mass loss. Sci. Adv. 5 (9), eaao0834.

Laveuf, C., Cornu, S., 2009. A review on the potentiality of rare earth elements to trace pedogenetic processes. Geoderma 154 (1–2), 1–12.

Lepsch, I.F., 2016. 19 lições de Pedologia. Oficina de Textos.

Kosmulski, M., 2009. pH-dependent surface charging and points of zero charge. iv. update and new approach. J. Colloid Interface Sci. 337 (2), 439–448.

Peccerillo, A., Taylor, S., 1976. Geochemistry of eocene calc-alkaline volcanic rocks from the Kastamonu area, northern Turkey. Contrib. Miner. Petrol. 58 (1), 63–81.

W. V. Boynton, Chapter 3 - cosmochemistry of the rare earth elements: Meteorite studies, in: P. Henderson (Ed.), Rare Earth Element Geochemistry, Vol. 2 of Developments in Geochemistry, Elsevier, 1984, pp. 63–114.

Whitney, D.L., Evans, B.W., 2010. Abbreviations for names of rock-forming minerals. Am. Mineral. 95 (1), 185–187.